CHAPTER 4

THE MULTIPLY-UPSTREAM SEMI-LAGRANGIAN METHOD OF SIMULATING ADVECTION

4.1 INTRODUCTION

Analytic and numerical solutions of the Eulerian equations of hydrodynamics are limited in extent by the non-linear advection, or transport terms. Analytic solutions are difficult to obtain because the advection terms render the equations non-linear. Finite difference numerical solutions are readily derived in principle but are inaccurate because finite difference approximations of the advection terms can introduce errors in phase and amplitude (Crowley, 1968; Mesinger and Arakawa, 1976). In order to remain stable, Eulerian time schemes must satisfy the Courant-Friedrichs-Lewy (CFL) criterion that restricts the size of the time step used for a given spatial resolution and advecting wind.

A Lagrangian approach to solving the equations of fluid motion involves following a fixed set of particles throughout the period of integration. However, Welander (1955) indicated that, in general, a set of fluid particles which are initially regularly distributed soon become significantly deformed and are therefore rendered unsuitable for numerical integration. To avoid this difficulty, while still concentrating on fluid particles, Wiin-Nielsen (1959) introduced a semi-Lagrangian approach, whereby a set of particles which arrive at a regular set of grid points are traced back over a single time interval to the location of the initial departure points. The values of the dynamical quantities at the departure points are obtained by interpolation from neighbouring grid points with known values. The semi-Lagrangian approach differs from the Lagrangian approach because in the former the set of particles in question changes at each time step.

In multiply-upstream semi-Lagrangian schemes the grid points used for interpolation to the departure point of a particle are selected in such a way that they always surround the departure point. When the winds are strong the set of grid points may be many grid intervals upstream from the arrival grid point. The term "multiply-upstream" is used to describe a scheme using interpolation points selected in this way (Bates and McDonald, 1982).

During the last fifteen years there has been an increased interest in semi-Lagrangian techniques to manipulate horizontal or vertical advection in numerical prediction models. The essential feature of such schemes is that the total or material derivatives in the equations of motion are treated directly by calculating the departure points of fluid parcels. The upstream value of the required fields are then usually evaluated by spatial interpolation (McGregor, 1993). The main advantage of semi-Lagrangian techniques is that it allows for the relaxation of the CFL criterion. The popularity of the semi-Lagrangian

approach stems however not only from the large permissible time steps but also from the high degree of advection accuracy. The schemes may be either two-time level or three-time level.

This chapter deals with the semi-Lagrangian method of numerically modelling the advective process. The goal is to clarify and elaborate upon some of the theoretical issues of semi-Lagrangian advection and to compare the semi-Lagranian scheme used in DARLAM to well-tested Eulerian schemes in order to evaluate their relative merits with respect to stability and accuracy.

4.2 THE ADVECTION EQUATION

In order to examine the properties of numerical advection schemes, numerical approximations to the two–dimensional advection equation in Cartesian co-ordinates will be analysed. The horizontal (two-dimensional) *non-linear* advection equation may be expressed as:

$$\frac{\partial \psi}{\partial t} + u\frac{\partial \psi}{\partial x} + v\frac{\partial \psi}{\partial y} = 0 \qquad \textbf{(4.1)}$$

Here $u = u(x, y, t)$ and $v = v(x, y, t)$ are the advection velocity components in the x and y directions respectively and t is time. The dependant variable $\psi = \psi(x, y, t)$ is some property (for example non-diffusive moisture) of the fluid that is transported by the flow field, so that its total derivative along an instantaneous streamline is zero. That is, equation **(4.1)** when written with respect to an observer who moves with the fluid simplifies to

$$\frac{d\psi}{dt} = 0\,,\ \psi = \psi(x_0, y_0, t_0)$$

so that an observer will measure no change in ψ as time passes. Equation **(4.1)**, also called the colour equation, is considered in practise to be the most important part of the atmospheric governing equations (Mesinger and Arakawa, 1976).

The *linear* two-dimensional advection equation is

$$\frac{\partial \psi}{\partial t} + u\frac{\partial \psi}{\partial x} + v\frac{\partial \psi}{\partial y} = 0\,; \qquad u,\ v \text{ constant} \qquad \textbf{(4.2)}$$

The *non-linear* advection equation in one space dimension is

$$\frac{\partial \psi}{\partial t} + u\frac{\partial \psi}{\partial x} = 0 \qquad \textbf{(4.3)}$$

where $\psi = \psi(x, t)$ and $u = u(x, t)$, while the *linear* advection equation in one space dimension is

$$\frac{\partial \psi}{\partial t} + u\frac{\partial \psi}{\partial x} = 0; \qquad u \text{ constant} \qquad \textbf{(4.4)}$$

Equation **(4.4)** describes the simplest advective processes and has proved to be a useful framework for the evaluation and comparison of numerical integration schemes.

Before investigating the properties of numerical solutions of the non-linear advection equation **(4.1)** it is useful to first obtain an analytical solution of the linear two-dimensional advection equation **(4.2)** in the form of a single harmonic

$$\psi(x, y, t) = \mathrm{Re}\left\{\Psi(t)e^{I(kx+ly)}\right\} \qquad \textbf{(4.5)}$$

Here $\Psi(t)$ is the wave amplitude, and k and l are wave numbers in the x and y directions respectively. $k = \frac{2\pi}{L_x}$ and $l = \frac{2\pi}{L_y}$ with L_x and L_y the wavelengths in the x and y directions respectively. The imaginary number I is defined as $I^2 \equiv -1$.

Substituting equation **(4.5)** into the linear advection equation **(4.2)** gives

$$\frac{d\Psi}{dt} + Iku\Psi + Ilv\Psi = 0 \qquad \textbf{(4.6)}$$

Thus, the problem of solving the partial differential equation **(4.2)** has been reduced to that of solving an ordinary differential equation **(4.6)** with the following solution:

$$\Psi(t) = \Psi(0)e^{-I(ku+lv)t} \qquad \textbf{(4.7)}$$

$\Psi(0)$ denotes the initial value of the amplitude. Hence, the desired harmonic solution is

$$\psi(x, y, t) = \mathrm{Re}\left\{\Psi(0)e^{Ik(x-ut)+Il(y-vt)}\right\} \qquad \textbf{(4.8)}$$

Each wave component is advected at a constant velocity of $c = \sqrt{u^2 + v^2}$ in the x-y plane, with no changes in amplitude. Important features in the assessment of a numerical integration scheme are therefore the damping (if any) and the phase speed of a single harmonic.

The one-dimensional linear advection equation **(4.4)** also has a solutions in the form of a single harmonic component,

$$\psi(x, t) = \mathrm{Re}\left\{\Psi(t)e^{Ikx}\right\}$$

provided that

$$\frac{d\Psi}{dt} + Iku = 0 . \qquad \textbf{(4.9)}$$

The solution of equation **(4.9)** is

$$\Psi(t) = \Psi(0)e^{-Ikut} \qquad \textbf{(4.10)}$$

or, for discrete values $t = n\Delta t$ (n is the number of time steps and Δt the time interval),

$$\Psi^n = \Psi(n\Delta t) = \Psi(0)e^{-Ikun\Delta t} \qquad \textbf{(4.11)}$$

where $\Psi(0)$ is the initial value of the amplitude. In equation **(4.11)** $\omega = -ku\Delta t$ represents the change in argument (or phase change) of the **(4.11)** in a single time step Δt. This will obviously also be the phase change in time of the true solution of the linear one-dimensional advection equation.

4.3 EULERIAN SCHEMES TO SOLVE THE ADVECTION EQUATION

In this section some well-tested Eulerian schemes to solve the advection equation are formulated and their accuracy and stability properties are discussed.

4.3.1 LEAPFROG SCHEME

4.3.1.1 Construction of the leapfrog scheme

One of the most widely used numerical schemes to solve the advection equation is the leapfrog scheme. The scheme is obtained by replacing both the time and space derivatives in the advection equation by centred (second order accurate) finite difference approximations. The scheme is a three-level scheme, meaning that it relates the values of the dependant variable at three time levels.

Approximating the space derivatives in the two-dimensional linear advection equation **(4.2)** with standard second order accurate difference quotients (Mesinger and Arakawa, 1976) results in

$$\frac{\partial \psi_{i,j}}{\partial t} = -u\frac{\psi_{i+1,j} - \psi_{i-1,j}}{2\Delta x} - v\frac{\psi_{i,j+1} - \psi_{i,j-1}}{2\Delta y} . \qquad \textbf{(4.12)}$$

The co-ordinates of grid point (i,j) are given by $x = i\Delta x$ and $y = j\Delta y$ with Δx and Δy the spatial increments in the x and y directions respectively.

Approximate values for $\psi(i\Delta x, j\Delta y)$ are denoted by $\psi_{i,j}$. Centred differences are used for the time derivative, resulting in the following equation:

$$\psi_{i,j,k+1} = \psi_{i,j,k-1} - \Delta t\left[u\frac{\psi_{i+1,j,k} - \psi_{i-1,j,k}}{\Delta x} + v\frac{\psi_{i,j+1,k} - \psi_{i,j-1,k}}{\Delta y}\right] \quad \textbf{(4.13)}$$

The points in time where the numerical solution is computed for equation **(4.2)** are given by $t = k\Delta t$, with $k \geq 2$. The solution for time step $t = 1.\Delta t$ is approximated by using backward time differencing:

$$\psi_{i,j,1} = \psi_{i,j,0} - \Delta t\left[u\frac{\psi_{i+1,j,0} - \psi_{i-1,j,0}}{2\Delta x} + v\frac{\psi_{i,j+1,0} - \psi_{i,j-1,0}}{2\Delta y}\right]. \quad \textbf{(4.14)}$$

4.3.1.2 Amplitude accuracy

It is instructive to investigate the amplitude and phase properties of numerical solutions from the linear advection equation **(4.2)**. Von Neumann's, or the Fourier series method (Mesinger and Arakawa, 1976), is employed for this purpose. A solution of the linear advection equation can be expressed in the form of a Fourier series, where each harmonic component is also a solution (Mesinger and Arakawa, 1976). The stability of a single harmonic may be tested and stability of all admissible harmonics then constitutes a necessary condition for stability of the scheme (Mesinger and Arakawa, 1976).

It is worthwhile to note that when using a grid point method to numerically solve partial differential equations with wave-type solutions, it is impossible to resolve waves with wavelengths shorter than $\min\{2\Delta x, 2\Delta y\}$ (Mesinger and Arakawa, 1976).

Returning to the von Neumann method, a solution of the finite difference equation **(4.13)** can be derived by substituting a solution of the following form of a single harmonic into equation **(4.12)**:

$$\psi_{i,j}^{n} = \mathrm{Re}\left\{\Psi^{n} e^{I(ki\Delta x + lj\Delta y)}\right\} \quad \textbf{(4.15)}$$

This is analogue to solution **(4.8)** of the linear advection equation at discrete points $i\Delta x$, $j\Delta y$ and $n\Delta t$. Here Ψ^n represents the amplitude of the numerical solution at time level n. After some rearrangement, it follows that the single harmonic **(4.15)** is a solution of equation **(4.12)** provided that

$$\frac{d\Psi}{dt} = I\left(-\frac{u}{\Delta x}\sin k\Delta x - \frac{v}{\Delta y}\sin l\Delta y\right)\Psi \quad \textbf{(4.16)}$$

Approximating the time derivative in **(4.12)** with centred differences yields

$$\Psi^{n+1} = \Psi^{n-1} + 2I\left(-u\frac{\Delta t}{\Delta x}\sin k\Delta x - v\frac{\Delta t}{\Delta y}\sin l\Delta y\right)\Psi^n \qquad \textbf{(4.17)}$$

Equation **(4.17)** enables analyses explaining the behaviour of the amplitude Ψ^n with an increase in time step (n). The amplification factor $|\lambda|$ is defined as

$$\Psi^{n+1} \equiv \lambda\Psi^n \qquad \textbf{(4.18)}$$

Taking the absolute value on both sides yields

$$|\Psi^{n+1}| = |\lambda||\Psi^n|$$

For the stability of each harmonic solution **(4.15)**, it is required that

$$|\Psi^n| = |\lambda|^n|\Psi^0| < B$$

where B is a finite number. Taking the logarithm on both sides yields:

$$n\ln|\lambda| < B' \quad \text{where} \quad B' \equiv \ln\left(\frac{B}{|\Psi^0|}\right)$$

Thus, B' is a new constant. Since $t = n\Delta t$, the necessary condition for stability becomes

$$\ln|\lambda| < \frac{B'}{t}\Delta t \qquad \textbf{(4.19)}$$

Suppose that boundedness of the solution is required for a finite time t.

Condition **(4.19)** can then be written as

$$\ln|\lambda| \le O(\Delta t)$$

Defining $|\lambda| \equiv 1+\delta$ and in view of the power series expansion

$$\ln(1+\delta) = \sum_{n=0}^{\infty}\frac{(-1)^n}{n+1}\delta^{n+1} \quad \text{for} \quad -1 < \delta < 1$$

(Ellis and Gulick, 1994) it follows that the stability condition obtained is equivalent to

$$\delta \le O(\Delta t)$$

or

$$\frac{d|\lambda_1|}{dp} = 1 + \frac{p}{\sqrt{p^2 - 1}}$$

which is unbounded if $p \to 1$

From equation **(4.21)** follows that the stability criterion $|p| \leq 1$ has to be written as

$$\left| u\frac{\Delta t}{\Delta x}\sin k\Delta x + v\frac{\Delta t}{\Delta y}\sin l\Delta y \right| \leq 1$$

This must be true for all resolvable wavelengths, which are all admissible values of the wave numbers k and l. If only the cases where $\Delta x = \Delta y$ is considered, the condition simplifies to

$$c\frac{\Delta t}{\Delta x}\sqrt{(\sin k\Delta x)^2 + (\sin l\Delta x)^2} \leq 1$$

where $c = \sqrt{u^2 + v^2}$. Mesinger and Arakawa (1976) showed that the case where $\sin k\Delta x = \sin l\Delta x = 1$ does occur within the admissible range of wave numbers. Thus, if the two-dimensional linear advection equation **(4.2)** is approximated using the leapfrog finite difference scheme, the amplitude of a solution in the form of a single harmonic component will remain bounded if

$$c\frac{\Delta t}{\Delta x}\sqrt{2} \leq 1 \qquad \textbf{(4.23)}$$

This constitutes a necessary condition for the stability of the scheme and is commonly known as the CFL criterion.

4.3.1.3 Phase accuracy

In this section the phase properties of the leapfrog scheme is investigated by considering approximations to the solution of the less complex one-dimensional linear advection equation **(4.4)**. The von Neumann method involves defining the amplification factor λ as

$$\Psi^{n+1} \equiv \lambda\Psi^n$$

(equation **(4.18)**). λ can be written as

$$\lambda = |\lambda|e^{I\theta} \qquad \textbf{(4.24)}$$

Equation **(4.18)** and **(4.24)** yields that the amplitude of the numerical solution at any time step is given by (Mesinger and Arakawa, 1976)

$$\Psi^n = |\lambda|^n \Psi^0 e^{In\theta}$$

Comparing this with equation **(4.11)** reveals that θ represents the change in argument (phase change) the numerical solution at each time step (Mesinger and Arakawa, 1976).

It is of interest to consider the phase change of the numerical solution per time step (θ) relative to that of the true solution ($\omega = -ku\Delta t$) namely

$$R = \frac{\theta}{\omega}$$

If the phase change of the numerical solution (θ) per time step is equal to that of the true solution (ω), the relative phase change (R) is unity. However, an expression for the phase change (θ) of the numerical solution first needs to be derived. Using the notation (following Mesinger and Arakawa (1976))

$$\lambda \equiv \lambda_{re} + I\lambda_{im}$$

it follows from equation **(4.24)** that

$$\tan\theta = \frac{\lambda_{im}}{\lambda_{re}} \qquad \textbf{(4.25)}$$

or

$$R = \frac{1}{\omega}\tan^{-1}\left(\frac{\lambda_{im}}{\lambda_{re}}\right). \qquad \textbf{(4.26)}$$

It has been shown in section 4.3.1.2 that the leapfrog scheme is stable if $p \le 1$ for the linear two-dimensional advection equation **(4.2)**. The same condition applies when solving the linear one-dimensional equation **(4.4)** with the leapfrog scheme, but now $p = -u\frac{\Delta t}{\Delta x}\sin k\Delta x$. Substituting the two solutions for (λ) from equation **(4.22)** into equation **(4.26)**, indicates that the relative phase change of the leapfrog scheme is

$$R_1 = \frac{1}{\omega}\tan^{-1}\left(\frac{p}{\sqrt{1-p^2}}\right)$$

$$R_2 = \frac{1}{\omega}\tan^{-1}\left(\frac{-p}{\sqrt{1-p^2}}\right)$$

with the condition that $|p| < 1$ with $p = -u\frac{\Delta t}{\Delta x}\sin k\Delta x$ for the one-dimensional linear advection equation (compare this to equation **(4.21)**).

For $|p| = 1$ it follows from equation **(4.22)** that $\lambda_1 = \lambda_2 = Ip$, implying that both values of λ have imaginary parts only. Equation **(4.24)** yields, for $p = \pm 1$, that

$$R_1 = R_2 = \pm \frac{\pi}{2\omega}$$

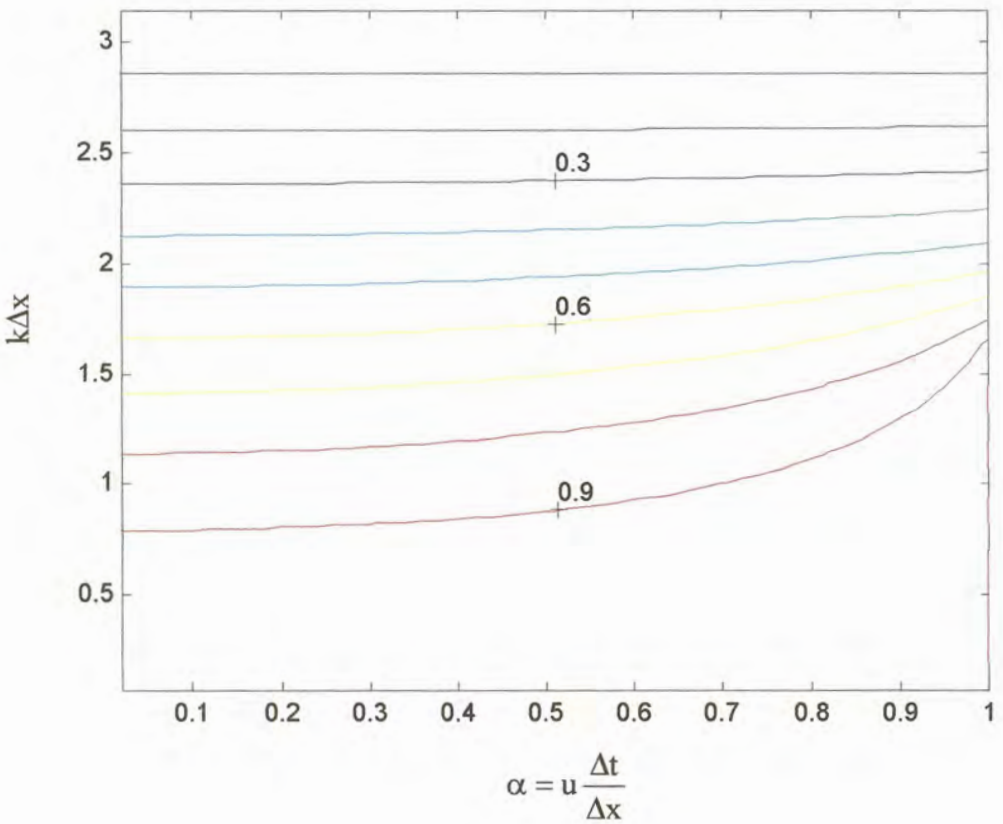

Figure 4.1 Relative phase speed isolines plotted as a function of $k\Delta x$ and α for the physical mode of the leapfrog scheme.

Relative phase speed isolines (R) are plotted in figure 4.1 for the physical mode for $0 \le k\Delta x \le \pi$ (admissible wave numbers) and $0 < \alpha = u\frac{\Delta t}{\Delta x} \le 1$ ($u\frac{\Delta t}{\Delta x} \le 1$ is the one-dimensional CFL criterion – analogue to equation **(4.23)**). It is obvious that the physical mode is decelerating ($R<1$) and that the deceleration increases as the wave number (k) increases. Also, the deceleration increases as α decreases. The relative phase speed of the computational mode is the same in magnitude as found for the physical mode but opposite in sign.

4.3.2 LAX-WENDROFF SCHEMES

4.3.2.1 Construction of the Lax-Wendroff and modified Lax-Wendroff schemes

Lax and Wendroff (1960) described an alternative finite difference method, which has since attracted considerable attention. For the linear two-dimensional advection equation **(4.2)** the Lax-Wendroff scheme is implemented as follows:

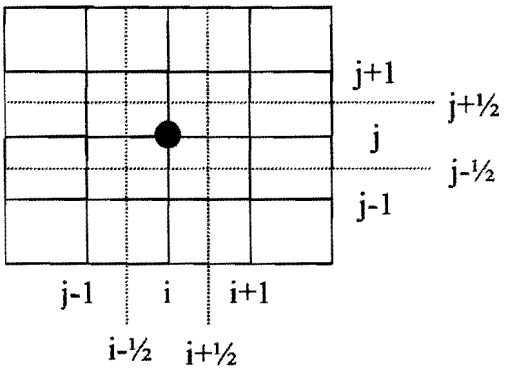

Figure 4.2 Grid configuration for the Lax-Wendrof scheme. The horizontal increment is Δx and the vertical increment is Δy.

Suppose the value of the dependant variable ψ needs to be updated at all grid points $(i\Delta x, j\Delta y)$ (circle in figure 4.2). First, provisional values for ψ at time step $n+\frac{1}{2}$ are calculated for all the "half points" at positions (x, y) with $x = \pm\left(i+\frac{1}{2}\right)\Delta x$ and $y = \pm\left(j+\frac{1}{2}\right)\Delta y$ (where the dotted lines cross in figure 4.2).

This is achieved by applying the following finite difference equation to each of the "half points":

$$\psi^{n+\frac{1}{2}} = \left(\psi^{xy}\right)^n - \frac{1}{2}\left\{\alpha_1\left(\delta_x\psi^y\right)^n + \alpha_2\left(\delta_y\psi^x\right)^n\right\} \qquad \textbf{(4.27)}$$

Equation **(4.27)** employs centred space (equations **(4.30a)** and **(4.30b)** with $m = 1$) and forward time differencing. α_1 and α_2 are given by **(4.31)**. It is necessary to take arithmetic averages in space when calculating the centred space differences (equations **(4.30a)** and **(4.30b)**) and when calculating ψ^n at a particular half point (equation **(4.29)**). Note that the "half points" used at time step n+½ are spatially staggered.

Using these provisional values a second step is taken, centred in both space and time, to update the values of the dependant variable (at time step n+1) at all grid points $x = i\Delta x$ and $y = j\Delta y$ (circle in figure 4.2):

$$\psi^{n+1} = \psi^{n} - \left\{ \alpha_1 \left(\delta_x \psi^{y}\right)^{n+\frac{1}{2}} + \alpha_2 \left(\delta_y \psi^{x}\right)^{n+\frac{1}{2}} \right\} \qquad \textbf{(4 .28)}$$

Note that

$$\left(\psi^{xy}\right)^{n} = \frac{\psi^{n}_{i-\frac{1}{2},j-\frac{1}{2}} + \psi^{n}_{i-\frac{1}{2},j+\frac{1}{2}} + \psi^{n}_{i+\frac{1}{2},j-\frac{1}{2}} + \psi^{n}_{i+\frac{1}{2},j+\frac{1}{2}}}{4}, \qquad \textbf{(4.29)}$$

$$\left(\delta_{mx} \psi^{y}\right)^{n} = \frac{\psi^{n}_{i+\frac{m}{2},j+\frac{1}{2}} + \psi^{n}_{i+\frac{m}{2},j-\frac{1}{2}}}{2m} - \frac{\psi^{n}_{i-\frac{m}{2},j+\frac{1}{2}} + \psi^{n}_{i-\frac{m}{2},j-\frac{1}{2}}}{2m} \qquad \textbf{(4.30a)}$$

$$\left(\delta_{my} \psi^{x}\right)^{n} = \frac{\psi^{n}_{i+\frac{1}{2},j+\frac{m}{2}} + \psi^{n}_{i-\frac{1}{2},j+\frac{m}{2}}}{2m} - \frac{\psi^{n}_{i+\frac{1}{2},j-\frac{m}{2}} + \psi^{n}_{i-\frac{1}{2},j-\frac{m}{2}}}{2m} \qquad \textbf{(4.30b)}$$

$$\alpha_1 = u\frac{\Delta t}{\Delta x} \quad \text{and} \quad \alpha_2 = v\frac{\Delta t}{\Delta y} \qquad \textbf{(4.31)}$$

Equations (4.27) to (4.31) constitute the Lax-Wendroff scheme. Note again that m=1 when using equations **(4.30a)** and **(4.30b)**. Similar to the leapfrog scheme, the Lax-Wendroff scheme is second-order-accurate in space and time (Gadd, 1978a). The Lax-Wendroff scheme is, however, a two-level scheme (involving only time steps n and n+1) whereas the leapfrog scheme is a three-level scheme (time step n-1 is also involved). Two-level schemes are more attractive, since no computational initial condition is required as for three-level schemes. Certain types of non-linear computational instability can be avoided for this reason (Morton, 1971). In practical situations two-level schemes lead to smaller requirements for computer storage and allow exact model restarts to be made from a single field (Gadd, 1978a).

The damping and phase errors of the Lax-Wendroff scheme have been studied by Morton (1971), who indicated that the phase performance is rather poor compared to the leapfrog scheme on a time-staggered grid. Without time staggering the phase lag errors of the two schemes are similar (Gadd, 1978a).

Gadd (1978a) illustrated that a simple and inexpensive modification to the Lax-Wendroff scheme may result in a scheme with substantially reduced phase speed errors. In this modified Lax-Wendroff scheme the first step (equation **(4.27)**) remains the same. In the second step four rather than two grid points are used in the finite difference approximation to the spatial derivatives. Thus, equation **(4.28)** is replaced by

$$\psi^{n+1} = \psi^n - (1+a)\left\{\alpha_1\left(\delta_x\psi^y\right)^{n+\frac{1}{2}} + \alpha_2\left(\delta_y\psi^x\right)^{n+\frac{1}{2}}\right\} + a\left\{\alpha_1\left(\delta_{3x}\psi^y\right)^{n+\frac{1}{2}} + \alpha_2\left(\delta_{3y}\psi^x\right)^{n+\frac{1}{2}}\right\} \quad \textbf{(4.32)}$$

where $a \geq 0$ on intuitive grounds (Gadd, 1978a)

Equation **(4.32)** remains a second order accurate approximation in space and time (Gadd, 1978a). Equations **(4.29)**, **(4.30a)** and **(4.30b)** and **(4.31)** are still applied.

The linear one-dimensional advection equation **(4.4)** provides a useful framework for a theoretical analysis of the stability and phase properties of the Lax-Wendroff schemes. In the one-dimensional case the schemes are constructed in exactly the same way as for the two-dimensional equation:

First, provisional values for the dependant variable ψ at time step $n+\frac{1}{2}$ are calculated at all "half points" $x = \left(i \pm \frac{1}{2}\right)\Delta x$. This is achieved by using

$$\psi_{i+\frac{1}{2}}^{n+\frac{1}{2}} = \left(\psi^x\right)_{i+\frac{1}{2}}^n - \frac{1}{2}\alpha\left(\delta_x\psi\right)_{i+\frac{1}{2}}^n \quad \textbf{(4.33)}$$

Secondly, the values of the dependant variable (at time level n) is updated at all points $x = i\Delta x$

$$\psi_i^{n+1} = \psi_i^n - \alpha\left\{(1+a)\left(\delta_x\psi\right)_i^{n+\frac{1}{2}} - a\left(\delta_{3x}\psi\right)_i^{n+\frac{1}{2}}\right\} \quad \textbf{(4.34)}$$

Note that

$$\left(\psi^x\right)_i^n = \frac{\psi_{i-\frac{1}{2}}^n + \psi_{i+\frac{1}{2}}^n}{2} \quad \textbf{(4.35)}$$

and

$$\left(\delta_{mx}\psi\right)_i^n = \frac{\psi_{i+\frac{m}{2}}^n - \psi_{i-\frac{m}{2}}^n}{m} \quad \textbf{(4.36)}$$

As previously mentioned $\alpha = u\frac{\Delta t}{\Delta x}$

Note that $a \geq 0$. Also keep in mind that $a = 0$ reduces to the original Lax-Wendroff scheme. Equations **(4.33)** and **(4.34)** may be combined (Gadd, 1978a) to give

$$\psi_i^{n+1} = \psi_i^n - \alpha\left\{\left(1+\frac{2}{3}a\right)\left(\delta_{2x}\psi\right)_i^n - \frac{2}{3}a\left(\delta_{4x}\psi\right)_i^n\right\} + \frac{1}{2}\alpha^2\left\{\left(1+\frac{4}{3}a\right)\left(\delta_x^2\psi\right)_i^n - \frac{4}{3}a\left(\delta_{2x}^2\psi\right)_i^n\right\} \quad \textbf{(4.37)}$$

4.3.2.2 Amplitude accuracy

The phase and amplitude properties of equation **(4.37)** may be investigated by considering a single Fourier harmonic, with the discrete equivalent in the form of $\psi_i^n = \mathrm{Re}\left\{\Psi^n e^{I(ki\Delta x)}\right\}$. Keeping in mind relationship **(4.18)**, substitution of the Fourier harmonic into equation **(4.37)** yields Gadd (1978a):

$$\lambda(\alpha, k) = 1 - 2\alpha^2\left(\sin\frac{k\Delta x}{2}\right)^2\left[1+\frac{4}{3}a\left(\sin\frac{k\Delta x}{2}\right)^2\right] - 2I\alpha\left(\sin\frac{k\Delta x}{2}\right)\left(\cos\frac{k\Delta x}{2}\right)\left[1+\frac{4}{3}a\left(\sin\frac{k\Delta x}{2}\right)^2\right] \quad \textbf{(4.38)}$$

Thus, the amplitude of the Fourier harmonic is damped by a factor $|\lambda|$ at each time step. For computational stability it is required that $|\lambda| \leq 1$ for all wave numbers k. Taking absolute values on both sides of equation **(4.38)** and squaring gives

$$|\lambda|^2 = 1 - 4\alpha^2\left(\sin\frac{k\Delta x}{2}\right)^4\left(1+\frac{4}{3}a\left(\sin\frac{k\Delta x}{2}\right)^2\right)\left\{\left(1-\alpha^2\right)\left[1+\frac{4}{3}a\left(\sin\frac{k\Delta x}{2}\right)^2\right] - \frac{4}{3}a\right\} \quad \textbf{(4.39)}$$

which yields the computational stability criterion

$$\left(1-\alpha^2\right)\left[1+\frac{4}{3}a\left(\sin\frac{k\Delta x}{2}\right)^2\right] - \frac{4}{3}a \geq 0 \quad \textbf{(4.40)}$$

When $a = 0$ (Lax-Wendroff scheme) condition **(4.40)** reduces to $\alpha \leq 1$ which is the well-known CFL criterion. For $a = \frac{1}{2}$ condition **(4.40)** reduces to the less generous $\alpha \leq \frac{1}{3}$. This is unacceptable in numerical models where the time step is dictated by the wind speed (Gadd, 1978a) because the calculations are too expensive due to the small time step required to meet the stability

criterion. Therefore, a condition is required on a that ensures that $\alpha \leq 1$ remains a sufficient condition for stability.

The most restrictive case in equation **(4.40)** is that of $\frac{k\Delta x}{2} = 0$ so that the required condition is $a \leq \frac{3}{4}(1-\alpha^2)$. In the scheme proposed by Gadd (1978a) the limiting form of a, namely $a = \frac{3}{4}(1-\alpha^2)$ was adopted.

Lines of constant $|\lambda(\alpha, k)|$ are displayed in figure 4.3 ($a = 0$, Lax-Wendroff scheme) and figure 4.4 ($a = \frac{3}{4}(1-\alpha^2)$, modified Lax-Wendroff scheme), for $0 \leq k\Delta x \leq \pi$ and $0 \leq \alpha \leq 1$. Note that only solutions with wavelengths $L_x \geq 2\Delta x$ can be resolved, therefore only wave numbers $k\Delta x \leq \pi$ are admissible.

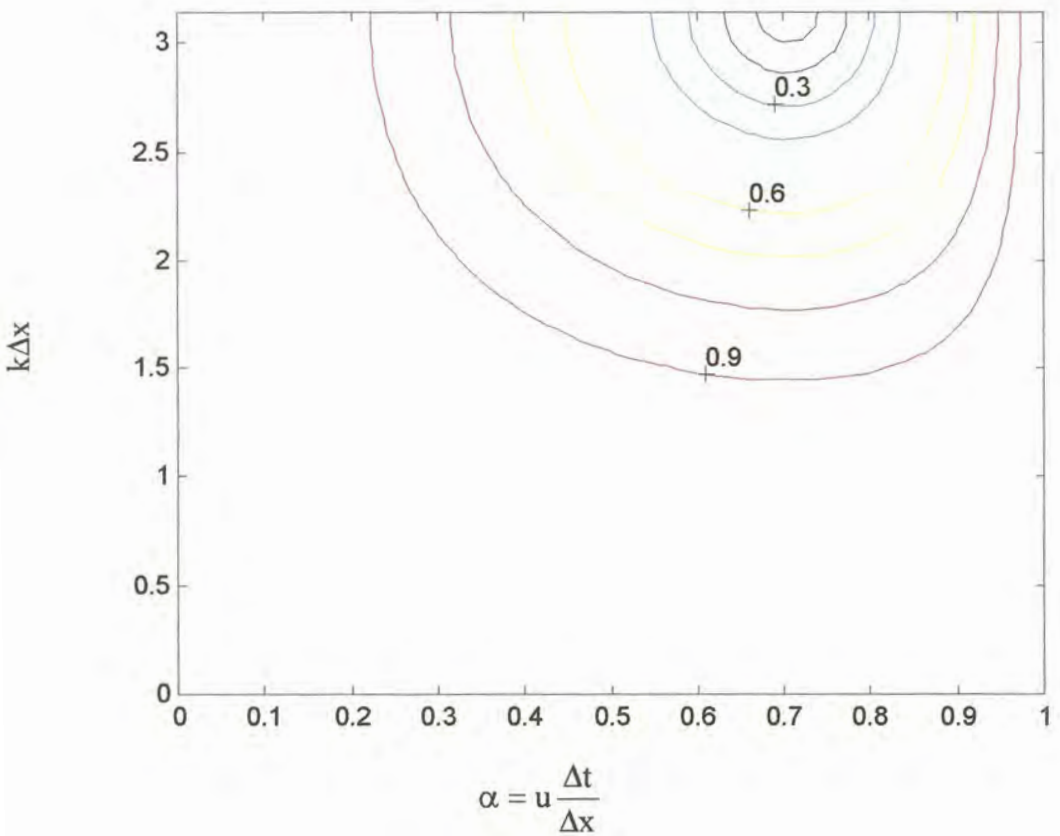

Figure 4.3 Isolines of the amplification factor plotted as a function of $k\Delta x$ and α for the Lax-Wendroff scheme.

In both schemes the damping is most noticeable for the shortest resolvable wavelengths and it decreases as the wavelength increases. Both schemes are undamped when $\alpha = 0.0$ or $\alpha = 1.0$. The Lax-Wendroff scheme is most severely damped when α is close to 0.7 but for the modified Lax-Wendroff scheme most of the damping occurs when α is between 0.5 and 0.6. The modified Lax-Wendroff scheme is the significantly less damped of the two

schemes. This represents an improvement of the modified Lax-Wendroff scheme over the Lax-Wendroff scheme.

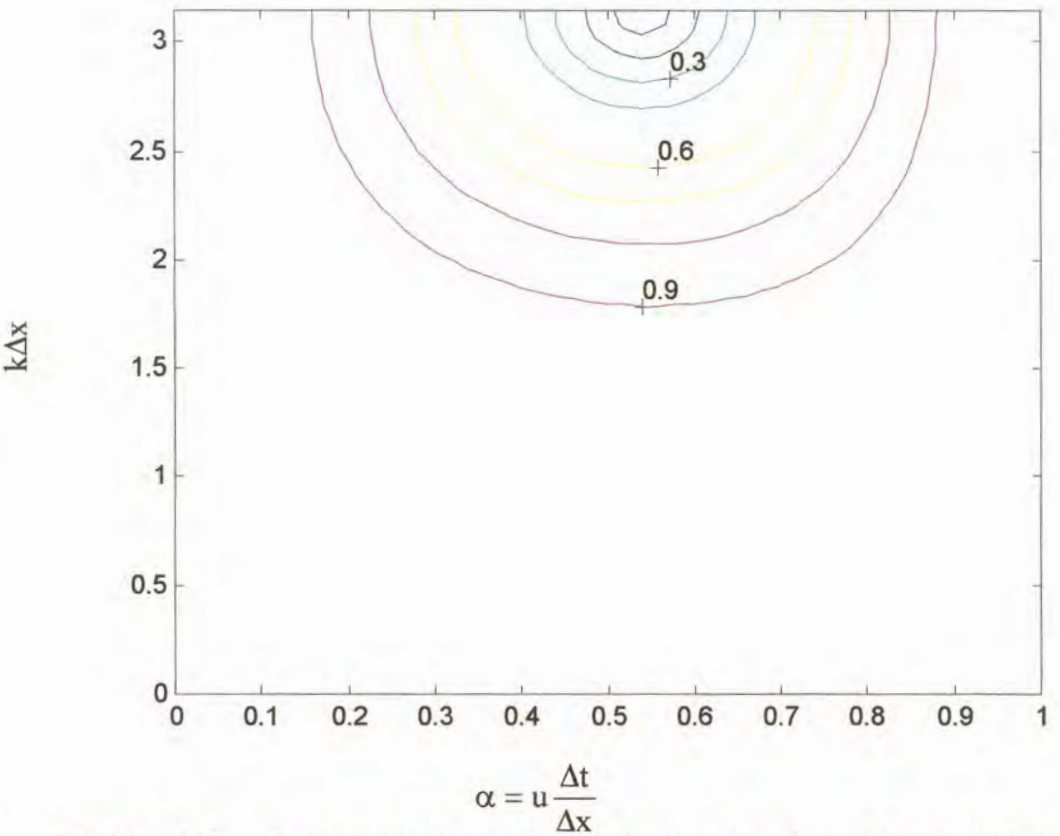

Figure 4.4 Isolines of the amplification factor plotted as a function of $k\Delta x$ and α for the modified Lax-Wendroff scheme.

The stability properties of the two-dimensional Lax-Wendroff schemes correspond closely to those of the one-dimensional schemes. For the two-dimensional version of the scheme $a = \frac{3}{4}(1-\chi^2)$ is chosen (Gadd, 1978a) where $\chi^2 = \alpha_1^2 + \alpha_2^2$.

Writing

$\alpha_1 = \chi\cos\phi$, $\alpha_2 = \chi\sin\phi$ and $d_x = \frac{1}{2}k\Delta x$, $d_y = \frac{1}{2}l\Delta y$

where k and l are wavenumbers in the x and y directions, it may be shown (Gadd, 1978a) that the application of equations (4.27), (4.28) and (4.31) to a typical Fourier mode yields a amplification factor of

$$\lambda(d_x, d_y, \chi, \phi) = 1 - 2\chi^2 A\{A + (1-\chi^2)B\} - 2I\chi\eta\{A + (1-\chi^2)B\}$$

where

$$A = \cos\phi \sin d_x \cos d_y + \sin\phi \cos d_x \sin d_y$$

$$B = \cos\phi \sin^3 d_x \cos d_y + \sin\phi \cos d_x \sin^3 d_y$$

and $\eta = \cos d_x \cos d_y$

It may be shown that $|\lambda| \leq 1$ provided that $\chi^2 \leq 1$ (Gadd, 1978a), which is the same as the necessary computational stability criterion for linear two-dimensional advection of the ordinary Lax-Wendroff scheme (Gadd, 1978a). For the special event where $\Delta x = \Delta y$ the necessary condition for stability simplifies to

$$c\frac{\Delta t}{\Delta x} \leq 1 \qquad \textbf{(4.41)}$$

Note that this is more generous than the typical two-dimensional CFL condition **(4.23)** as a result of the averaging operators in **(4.27)** and **(4.28)** (Gadd, 1978a).

4.3.2.3 Phase accuracy

From equations **(4.26)** and **(4.38)** it follows that, when the one-dimensional Lax-Wendroff schemes are applied to the linear advection equation **(4.4)**,

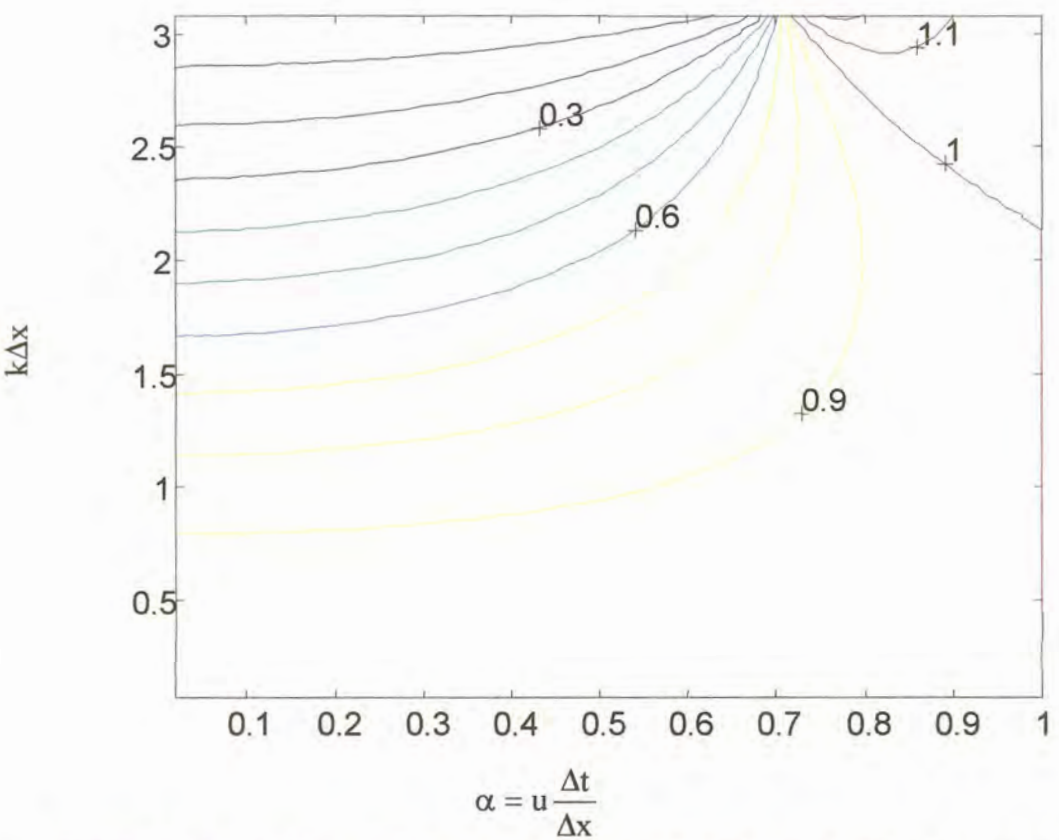

Figure 4.5 Relative phase speed isolines plotted as a function of $k\Delta x$ and α for the Lax-Wendroff scheme.

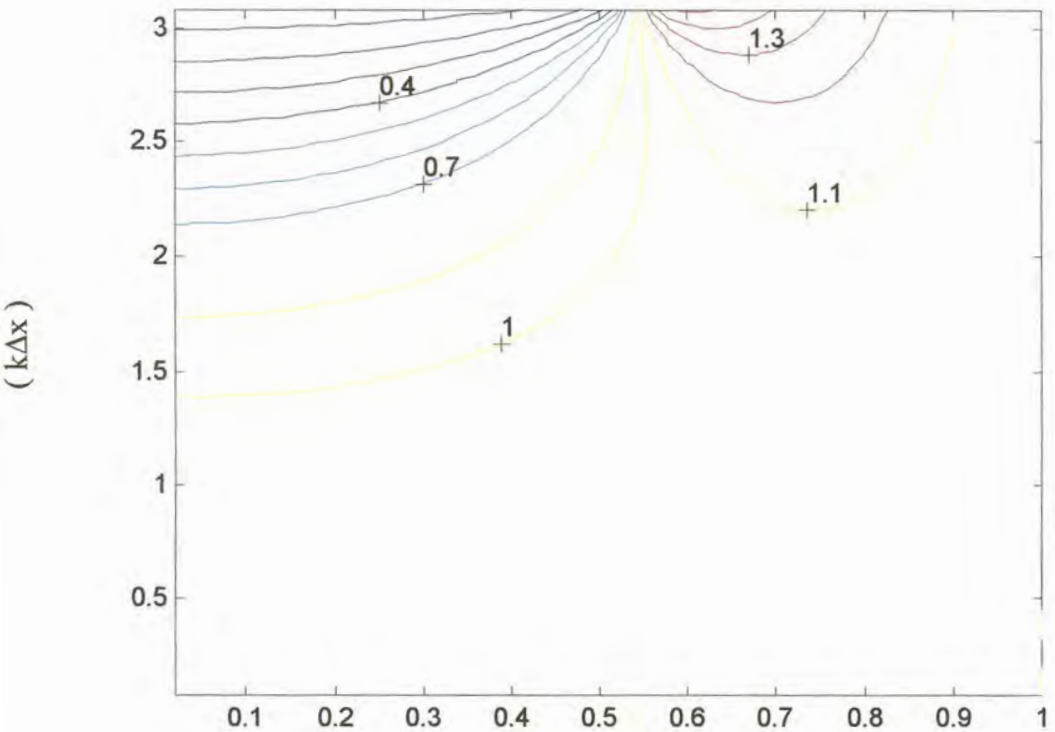

Figure 4.6 Relative phase speed isolines plotted as a function of $k\Delta x$ and α for the modified Lax-Wendroff scheme.

$$R(\alpha,k)=\frac{1}{\omega}\tan^{-1}\left\{\frac{-2\alpha\left(\sin\frac{k\Delta x}{2}\right)\left(\cos\frac{k\Delta x}{2}\right)\left[1+\frac{4}{3}a\left(\sin\frac{k\Delta x}{2}\right)^2\right]}{1-2\alpha^2\left(\sin\frac{k\Delta x}{2}\right)^2\left[1+\frac{4}{3}a\left(\sin\frac{k\Delta x}{2}\right)^2\right]}\right\} \qquad \textbf{(4.42)}$$

Relative phase speed isolines are plotted in figure 4.5 (Lax-Wendroff scheme) and figure 4.6 (modified Lax-Wendroff scheme) for $0 \le k\Delta x < \pi$ (admissible wave numbers) and $0 \le \alpha = u\frac{\Delta t}{\Delta x} \le 1$ (the one-dimensional CFL-criterion, compare this to equation **(4.41)**)

The superior phase properties of the modified Lax-Wendroff scheme (compared to the Lax-Wendroff scheme (figure 4.5) and leapfrog scheme (figure 4.1)) are obvious from figure 4.6. Interesting to note is that for most values of α and k the numerical phase speed is slightly greater than the analytic phase speed, in contrast to the usual phase lag of finite difference models (Gadd, 1978a). Gadd (1978a) discusses the case where $k\Delta x = \pi$ (corresponding to the shortest resolvable wave). This wave either does not move at all or moves exactly one grid length in a time step. The transition

occurs when $\alpha^2 = 1 - \frac{1}{\sqrt{2}}$, which gives a singularity in R. Since this wave is not properly resolved (Gadd, 1978a) the strong damping visible in figures 4.5 and 4.6 at $k\Delta x = \pi$ is an advantage.

4.4 MCGREGOR'S SEMI-LAGRANGIAN ADVECTION SCHEME

4.4.1 MULTIPLY-UPSTREAM SEMI-LAGRANGIAN ADVECTION

In the semi-Lagrangian approach of numerically simulating advection, a set of particles which arrive at a regular set of grid points are traced back over a single time interval to their departure points. The values of the dynamical quantities at the departure points are obtained by interpolation from neighbouring grid points with known values. The essential feature of semi-Lagrangian numerical models is that the total, or material derivatives, in the equations of motion are treated directly by calculating the departure points of fluid parcels. The upstream value of the required fields are usually evaluated by spatial interpolation (McGregor, 1993).

In multiply-upstream semi-Lagrangian schemes the grid points used for interpolation to the departure point of a particle are chosen in such a way that they always surround the departure point. When the winds are strong, this set of grid points may be many grid intervals upstream from the arrival grid point of the particle. The term "multiply-upstream" is used to describe a scheme using interpolation points chosen in this way (Bates and McDonald, 1982).

4.4.2 MCGREGOR'S METHOD OF DETERMINING DEPARTURE POINTS

During an integration of the primitive equations using the multiply-upstream semi-Lagrangian approach, the departure point (x_*, y_*) of a particle in a velocity field $\bar{v} = (u, v)$ over a time interval Δt may be estimated in a variety of ways. A simple straight-line trajectory back in time using only the velocity at the arrival point possesses inadequate accuracy (Robert, 1982). Most schemes therefore involve a sequence of iterations. A first guess of the departure position is determined by using a straight-line trajectory and an estimation of the departure velocity is then found by horizontal interpolation at the central point of the trajectory. This process is repeated several times using an updated advection velocity (McDonald, 1987; McDonald and Bates, 1987, 1989). McGregor (1993) points out that a significant overhead of such schemes can arise from the horizontal interpolation (traditionally bicubic) that is carried out during the iterations. Several authors however, reported acceptable accuracy using just linear interpolation (Temperton and Staniforth, 1987; Bates et al., 1990).

McGregor (1993) derived a more economical method to determine the position of departure points that avoids horizontal interpolation in the trajectory

analysis. The method considers a set of vectors moving with the fluid where each vector will be associated at time t with a different grid point. Note that the grid points have fixed locations while the vectors move with the fluid. To advance the model integration from time t to time $t + \Delta t$, a vector $\bar{r}(t+\Delta t)$ is constructed at the position of each arrival grid point. It is required to identify a starting position for the vector at the preceding time step namely $\bar{r}(t)$. Each vector $\bar{r}(t)$ therefore represents a departure point in the form (x_*, y_*). The process may be expressed in terms of a truncated Taylor series (McGregor, 1993), namely

$$\bar{r}(t) \approx \bar{r}(t+\Delta t) + \sum_{n=1}^{N} \frac{(-\Delta t)^n}{n!} \frac{d^n \bar{r}}{dt^n}(t+\Delta t) \qquad \textbf{(4.43)}$$

where

$$\frac{d^n \bar{r}(t)}{dt^n} = \frac{d}{dt}\frac{d^{n-1}\bar{r}(t)}{dt^{n-1}} \qquad n = 2,3,\ldots N \qquad \textbf{(4.44)}$$

and the total derivative operator has the usual definition of a time derivative that follows the motion of a parcel,

$$\frac{d}{dt} = \frac{\partial}{\partial t} + \bar{v}\cdot\bar{\nabla}. \qquad \textbf{(4.45)}$$

An array of the vectors $\bar{r}(t+\Delta t)$ is needed so that the $\bar{v}\cdot\bar{\nabla}$ operator in equation **(4.45)** may be conveniently evaluated. $\bar{v} = \frac{d\bar{r}}{dt}$ is the velocity of the fluid at position $\bar{r}(t)$, and $\bar{\nabla}$ is the spatial gradient operator. In equation **(4.45)** the time derivative on the left-hand side is naturally viewed from a Lagrangian viewpoint. The right hand side allows for its instantaneous evaluation at the same point in time and space via Eulerian derivatives (McGregor, 1993). McGregor (1993) points out that in the above equations, each component of $\bar{r} = (x_*, y_*)$ may be obtained independently from the others.

If the Eulerian velocity changes with time it becomes difficult, or at least very cumbersome, to evaluate the partial time derivatives for the higher order terms at $t+\Delta t$. In the scheme proposed by McGregor (1993) the total time derivative in **(4.45)**, for use in **(4.43)** and **(4.44)**, is replaced by the following approximation:

$$\frac{d}{dt} \approx \hat{v}\cdot\bar{\nabla}. \qquad \textbf{(4.46)}$$

Here $\hat{v}$ represents the Eulerian velocity at the point in space which corresponds to $\bar{r}(t+\Delta t)$, but is evaluated at the intermediate time $t+\frac{\Delta t}{2}$

(McGregor, 1993). The velocity $\hat{v}$ may conveniently be determined from the known velocities at previous time steps (McGregor, 1993). Temperton and Staniforth (1987), suggested the following third-order accuracy formulation in time:

$$\hat{v} = \frac{1}{8}\left[15\bar{v}(t) - 10\bar{v}(t-\Delta t) + 3\bar{v}(t-2\Delta t)\right] + O\left(\Delta t^3\right)$$

From an Eulerian point of view, approximation **(4.46)** suggests that for advection purposes, the velocities remain constant at their centred-in-time values over the time interval $[t, t+\Delta t]$ (McGregor, 1993).

The above scheme, using equations **(4.43)**, **(4.44)** and **(4.46)** and retaining terms up to the N^{th} total time derivative, is called a D_N scheme (McGregor, 1993). Equation **(4.46)** indicates that the lowest-order D_1 scheme only produces a straight-line trajectory, using a velocity $\hat{v}$ evaluated at the arrival position. The D_2 scheme uses estimates for both the velocity and acceleration along the trajectory. The D_3 and higher-order versions of the scheme effectively solve the trajectory by incorporating higher-order curvature terms derived kinematically for the arrival point from the velocity field $\hat{v}$ at time $t+\frac{\Delta t}{2}$ (McGregor, 1993). The number of terms that should be retained in the Tailor series **(4.43)** depends on the smoothness of the velocity field (McGregor, 1993). McGregor (1993) mentions that only slight benefit has been found in going beyond the D_3 scheme. Above, the scheme description focuses on two time-level applications. This might be modified if three time-level applications are required (McGregor, 1993).

4.4.3 INTERPOLATION

Approximating the non-linear or linear two-dimensional advection equation according to the semi-Lagrangian philosophy yields

$$\psi\{I_*\Delta x, J_*\Delta y, (n+1)\Delta t\} = \psi\{x_*, y_*, n\Delta t\}. \qquad \textbf{(4.47)}$$

Here (x_*, y_*) denote the position of the departure point for the arrival grid point $(I_*\Delta x, J_*\Delta y)$. Introducing the notation $\psi^n_{I_*,J_*} = \psi(I_*\Delta x, J_*\Delta y, n\Delta t)$, the function $\psi(x_*, y_*, t)$ is approximated by a Lagrange interpolating polynomial (Carnahan et al., 1969) using values of ψ at the grid positions nearest to x_* and y_*:

$$\psi(x_*, y_*, t) = \sum_{\mu}\sum_{\nu} W_{\mu\nu}\psi^n{}_{\mu\nu} \qquad \textbf{(4.48)}$$

where

$$W_{rs} = \prod_{\mu \neq r} \frac{(x_* - x_\mu)}{(x_r - x_\mu)} \prod_{\nu \neq s} \frac{(y_* - y_\nu)}{(y_s - y_\nu)} \qquad \textbf{(4.49)}$$

McDonald (1984) investigated the relative merits of bilinear, biquadratic, bicubic and biquartic interpolation schemes to approximate $\psi(x_*, y_*, t)$ for constant in time velocity fields. The semi-Lagrangian scheme used by McDonald closely relates to the D1 scheme (the schemes are identical for constant in time velocity fields). McDonald (1984) found that bicubic interpolation gives the best phase representation of the true solution and bicuartic interpolation the most faithful amplitude representation. In DARLAM, bicubic interpolation is employed.

The subscripts μ and ν range over the points being used in the bicubic interpolation as:

$$\mu : i-2, i-1, i, i+1 \qquad \upsilon : j-2, j-1, j, j+1 \qquad \textbf{(4.50)}$$

The points (i, j) are chosen for the bicubic interpolation such that

$$(i-1)\Delta x < x_* \leq i\Delta x \qquad (j-1)\Delta y < y_* \leq j\Delta y \qquad \textbf{(4.51)}$$

4.4.4 AMPLITUDE ACCURACY

An investigation of the stability properties of multiply-upstream semi-Lagrangian schemes, when applied to the linear advection equation, reveals interesting properties. For the linear two-dimensional advection equation **(4.2)** or linear one-dimensional advection equation **(4.4)**, the velocity field is constant, so that $\frac{d\bar{r}^n}{dt^n}$ vanishes when $n \geq 2$. Thus, as indicated by equation **(4.43)** all the D_N schemes reduce to the D_1 scheme.

If α, $\hat{\alpha}$, β, and $\hat{\beta}$ are defined as

$$\alpha = u\frac{\Delta t}{\Delta x} \qquad \beta = v\frac{\Delta t}{\Delta y}$$
$$\hat{\alpha} = \alpha + i - I_* \qquad \hat{\beta} = \beta + j - J_* \qquad \textbf{(4.52)}$$

the selection of i and j in equation **(4.51)** guarantees that

$$0 \leq \hat{\alpha} < 1 \quad \text{and} \quad 0 \leq \hat{\beta} < 1 \qquad \textbf{(4.53)}$$

McDonald (1984) showed that these conditions are sufficient to ensure unconditional stability of his multiply-upstream semi-Lagrangian scheme when applied to the linear advection equation.

In order to examine the stability of the D_1 scheme with bicubic interpolation for constant advection velocity, a solution in the form of a single harmonic (equation **(4.15)**) is assumed and substituted into equation **(4.47)**. Equations **(4.48)** and **(4.49)** are used to evaluate $\psi(x_*, y_*, t)$.

First note that equation **(4.49)** can be written as

$$W_{rs} = \prod_{\mu \neq r} \frac{(x_* - x_\mu)}{(x_r - x_\mu)} \prod_{\nu \neq s} \frac{(y_* - y_\nu)}{(y_s - y_\nu)} = w_r w_s$$

where

$$w_r = \prod_{\mu \neq r} \frac{(x_* - x_\mu)}{(x_r - x_\mu)} \quad \text{and} \quad w_s = \prod_{\nu \neq s} \frac{(y_* - y_\nu)}{(y_s - y_\nu)}. \qquad \textbf{(4.54)}$$

Using equations **(4.50)**, **(4.51)** and **(4.52)** equation **(4.54)** can be written as

$$w_{i+r} = \prod_{\substack{\mu=-2 \\ \mu \neq r}}^{1} \frac{\hat{\alpha} + \mu}{\mu - r} \quad \text{and} \quad w_{j+s} = \prod_{\substack{\nu=-2 \\ \nu \neq s}}^{1} \frac{\hat{\beta} + \nu}{\nu - s} \qquad \textbf{(4.55)}$$

where the subscripts μ and ν range over the points: $\mu : -2,-1,0,1 \quad \nu : -2,-1,0,1$.
Substituting the harmonic into equation **(4.47)** yields

$$\psi_{I_*,J_*}^{n+1} = \sum_{\mu=-2}^{1} \sum_{\nu=-2}^{1} w_{i+\mu} w_{j+\nu} \psi_0 \lambda^n e^{I[(i+\mu)k\Delta x + (j+\nu)l\Delta y]}$$

This may be expressed as

$$\psi_{I_*,J_*}^{n+1} = \sum_{\mu=-2}^{1} \sum_{\nu=-2}^{1} w_{i+\mu} w_{j+\nu} \psi_0 \lambda^n e^{I(ik\Delta x + jl\Delta y)} e^{I\mu k\Delta x} e^{I\nu l\Delta y}.$$

Rearranging the terms gives

$$\psi_{I_*,J_*}^{n+1} = \left\{ \sum_{\mu=-2}^{1} w_{i+\mu} e^{I\mu k\Delta x} \sum_{\nu=-2}^{1} w_{i+\nu} e^{I\nu l\Delta y} \right\} \psi_0 \lambda^n e^{I(ik\Delta x + jl\Delta y)}$$

Substitution of equation **(4.55)** into the last equation gives

$$\psi_{I_*,J_*}^{n+1} = \left\{ \sum_{\substack{\mu=-2 \\ r \neq \mu}}^{1} \prod_{r=-2}^{1} \frac{\hat{\alpha} + r}{r - \mu} e^{I\mu k\Delta x} \sum_{\substack{\nu=-2 \\ s \neq \nu}}^{1} \prod_{s=-2}^{1} \frac{\hat{\beta} + s}{s - \nu} w_{i+\nu} e^{I\nu l\Delta y} \right\} \psi_0 \lambda^n e^{I(ik\Delta x + jl\Delta y)}$$

Thus, λ splits into the product of a "x-amplification factor" and "y-amplification factor" (McDonald, 1984) in the following way:

$$\lambda = \hat{\Lambda}(\hat{\alpha}, k)\hat{\Lambda}(\hat{\beta}, l),$$

where

$$\hat{\Lambda}(\hat{\alpha}, k) = \sum_{\substack{\mu=-2 \\ r\neq\mu}}^{1}\prod^{1}\frac{\hat{\alpha}+r}{r-\mu}e^{I\mu k\Delta x} \quad \text{and} \quad \hat{\Lambda}(\hat{\beta}, l) = \sum_{\substack{\nu=-2 \\ s\neq\nu}}^{1}\prod^{1}\frac{\hat{\beta}+s}{s-\nu}e^{Il\nu\Delta y}.$$

This makes the analysis particularly simple. A scheme is stable if both $\left|\hat{\Lambda}(\hat{\alpha}, k)\right| \leq 1$ and $\left|\hat{\Lambda}(\hat{\beta}, l)\right| \leq 1$ since it guarantees that $|\lambda \leq 1|$. A little bit of algebra shows that (McDonald, 1984):

$$\hat{\Lambda}(\hat{\alpha}, k) = \left[1 - c\hat{\alpha}^2 - \frac{c^2\hat{\alpha}(1-\hat{\alpha}^2)}{3}\right] + I\hat{\alpha}\sin(k\Delta x)\left[1 + \frac{c(1-\hat{\alpha}^2)}{3}\right] \qquad \textbf{(4.56)}$$

where $c = 1 - \cos(k\Delta x)$. This yields

$$\left|\hat{\Lambda}(\hat{\alpha}, k)\right|^2 = 1 - \frac{\hat{\alpha}(2-\hat{\alpha})(1-\hat{\alpha}^2)c^2[3 + 2c\hat{\alpha}(1-\hat{\alpha})]}{9} \qquad \textbf{(4.57)}$$

As can be shown, $\left|\hat{\Lambda}(\hat{\alpha}, k)\right| \leq 1$ as long as $0 \leq \hat{\alpha} \leq 1$. Similarly, $\left|\hat{\Lambda}(\hat{\beta}, l)\right| \leq 1$ for $0 \leq \hat{\beta} < 1$ as can be seen by replacing $\hat{\alpha}$ and k with $\hat{\beta}$ and l in equation **(4.57)**. Hence the scheme is unconditionally stable since conditions applicable to $\hat{\alpha}$ and $\hat{\beta}$ are guaranteed by the choice of interpolation grid points given in **(4.51)**.

Following McDonald (1984) the quantities $\hat{\alpha}$ and $\hat{\beta}$ can also be expressed in the bicubic interpolation schemes as

$$\hat{\alpha} = \alpha - [\alpha] \quad \text{if } \alpha \geq 0$$
$$\hat{\alpha} = \alpha - [\alpha - 1] \quad \text{if } \alpha < 0$$

Here, $[x]$ is the integer part of x, $\hat{\beta}$ is defined in exactly the same way as $\hat{\alpha}$ with β replacing α in all the above equations. Substituting these values of $\hat{\alpha}$ in equation **(4.57)** gives a function $|\Lambda(\alpha, k)| = \left|\hat{\Lambda}(\hat{\alpha}, k)\right|$ with the property that

$$|\Lambda(\alpha + n, k)| = |\Lambda(\alpha, k)| \qquad \textbf{(4.58)}$$

where n represents any integer.

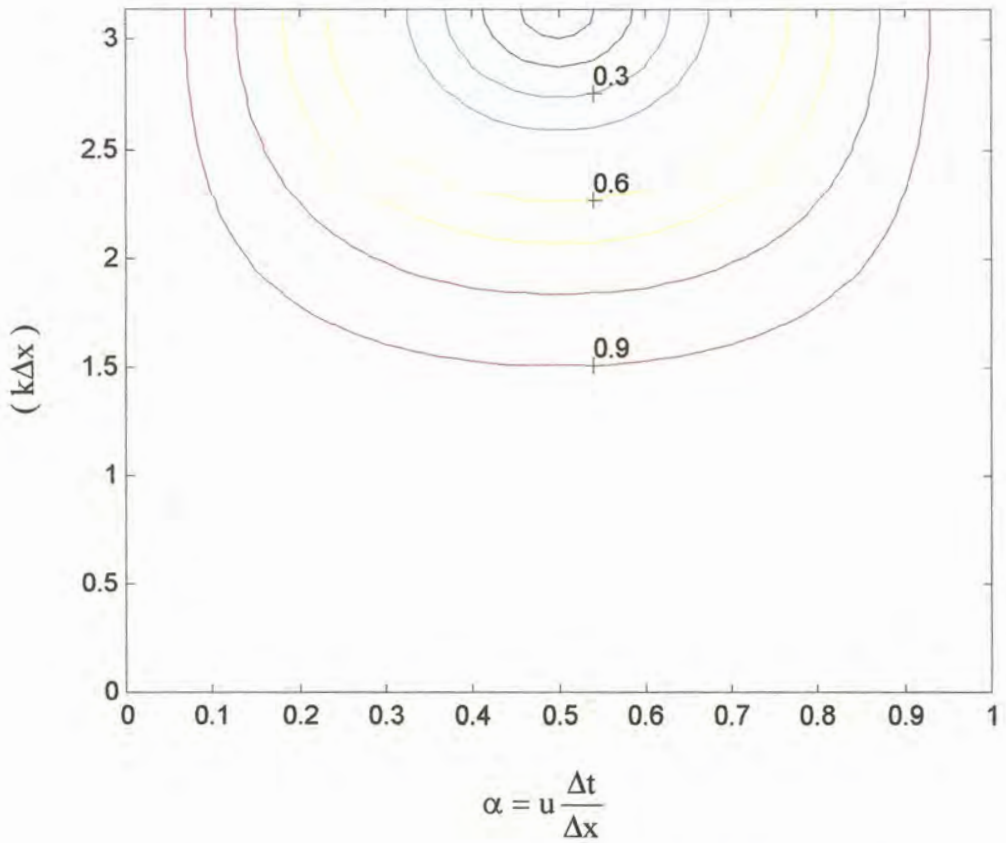

Figure 4.7 Isolines of the amplification factor plotted as a function of $k\Delta x$ and α for the D_1 scheme.

The lines of constant $|\Lambda(\alpha, k)|$ are displayed in figure 4.7 for $0 \leq k\Delta x < \pi$ (the admissible wave numbers) and $0 < \alpha \leq 1$. Equation **(4.58)** ensures that the graphs for all other regions $n < \alpha \leq n+1$ are identical to the graph illustrated in figure 4.7. Note that for the one-dimensional linear advection equation **(4.4)** it applies that $|\lambda(\hat{\alpha}, k)| = |\hat{\Lambda}(\hat{\alpha}, k)|$, so that figure 4.8 is directly comparable to figures 4.3 and 4.4.

The D_N schemes with bicubic interpolation are most severely damped when $\alpha = 0.5$ and undamped when $\alpha = 0$ or $\alpha = 1$. The damping is the most noticeable at the shortest resolvable wavelengths and it decreases as the wavelength increases. The Lax-Wendroff scheme is most damped, followed by the D_N schemes with bicubic interpolation, modified Lax-Wendroff and leapfrog schemes. No damping is present in the leapfrog scheme as long as the CFL criterion (equation **(4.23)**) applies.

4.4.5 PHASE ACCURACY

From equations **(4.26)** and **(4.56)** and for the D_1 scheme with bicubic interpolation (in one spatial dimension), it follows that:

$$R(\alpha,k)=\frac{-1}{\omega}\tan^{-1}\left\{\frac{\hat{\alpha}\sin(k\Delta x)\left[1+\frac{c(1-\hat{\alpha}^2)}{3}\right]}{\left[1-c\hat{\alpha}^2-\frac{c^2\hat{\alpha}(1-\hat{\alpha}^2)}{3}\right]}\right\}$$

Relative phase speed isolines are plotted in figure 4.9 for the D_1 scheme where $0\le k\Delta x\le\pi$ (admissible wave numbers) and $0<\alpha=u\frac{\Delta t}{\Delta x}\le 1$. The figure reveals that the D_1 scheme has the most realistic phase representation of all the schemes studied. A net phase lag occurs for $\alpha<\frac{1}{2}$ and there is a phase gain for $\frac{1}{2}<\alpha\le 1$

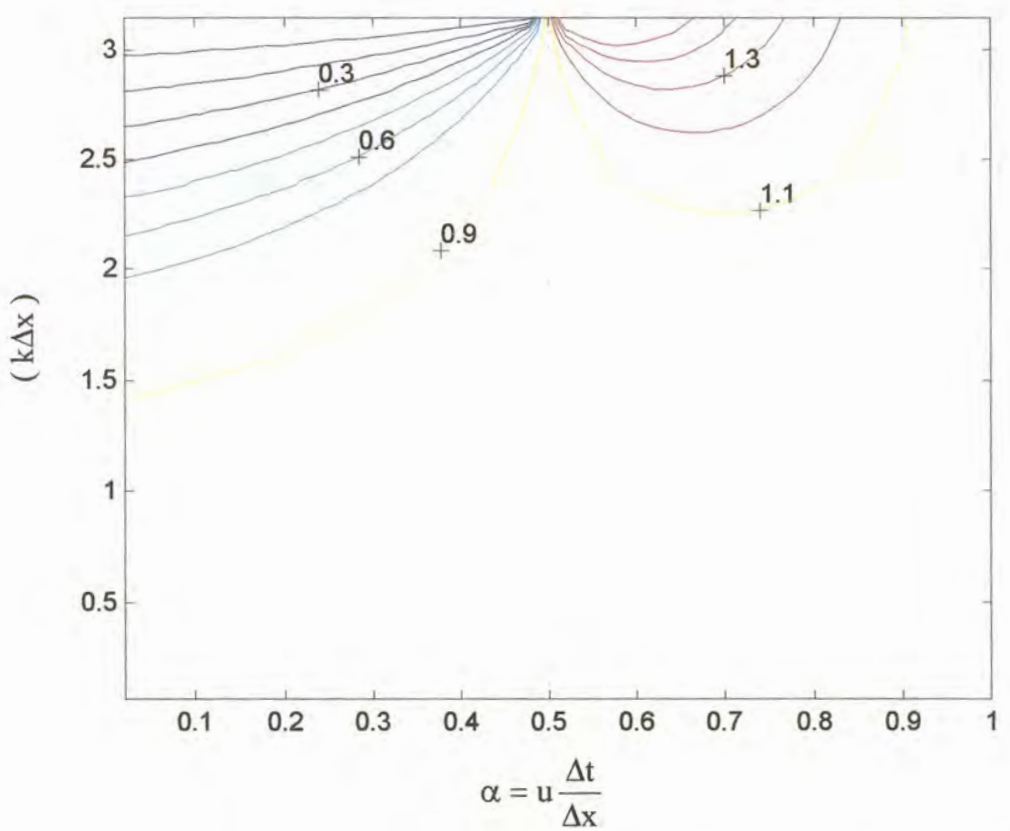

Figure 4.8 Relative phase speed isolines plotted as a function of $k\Delta x$ and α for the D_1 scheme.

4.5 TWO-DIMENSIONAL NUMERICAL TESTS

4.5.1 STEADY TWO-DIMENSIONAL FLOW: CROWLEY'S CONE TEST

In this section the accuracy and stability of the semi-Lagrangian D_1, D_2 and D_3 schemes are examined and compared to the Leapfrog and Lax-Wendroff finite difference schemes. The test problem used for this purpose is the advection of a cone at constant angular velocity about a point in the (x,y) plane, using the two-dimensional advection equation **(4.1)** (Crowley, 1968). The domain consists of 33x33 grid points covering the area $-16 \le x \le 16, -16 \le y \le 16$. An equation for the cone in its initial position, where the height ψ at any point is expressed as a function of x and y, is

$$\psi(x,y) = -25\sqrt{(x+8)^2 + y^2} + 100; \quad (x+8)^2 + y^2 \le 16$$

The cone therefore has an initial height of $\psi = 100$ units, a base diameter of 8 grid units and is initially centred at position $(-8,0)$. The domain configuration includes a buffer zone of one row around the lateral boundary where the height is held zero. These are the same settings as those used previously by McDonald (1984) and McGregor (1993).

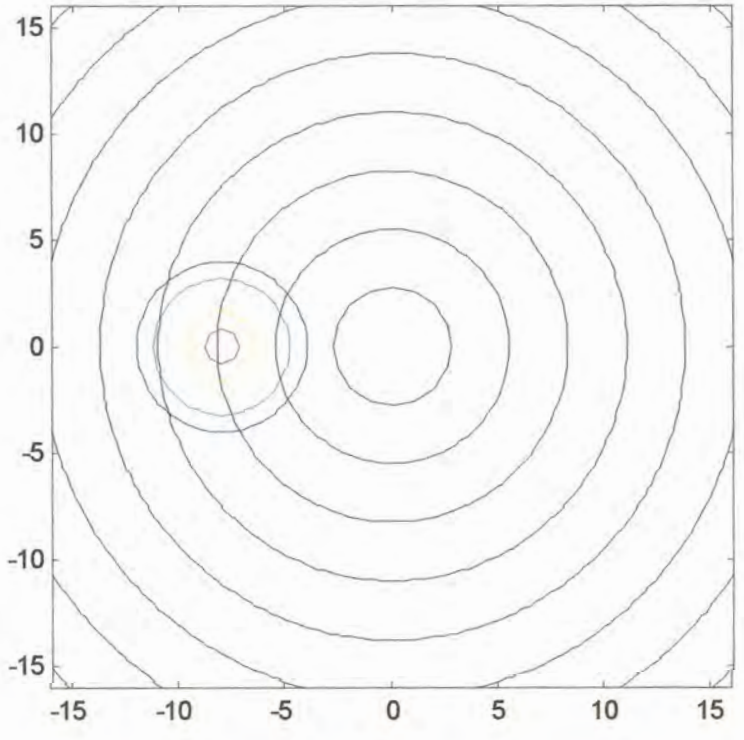

Figure 4.9 Isotachs of the velocity field (black contours) for Crowley's cone test with the initial cone location in colour. The cone has a height of 100 units, a base diameter of 8 units and is centred at position (-8,0).

The velocity field is given by

$$\bar{v} = (\Omega y, -\Omega x)$$

which constitutes steady two-dimensional solid-body rotation about the position $(0,0)$.

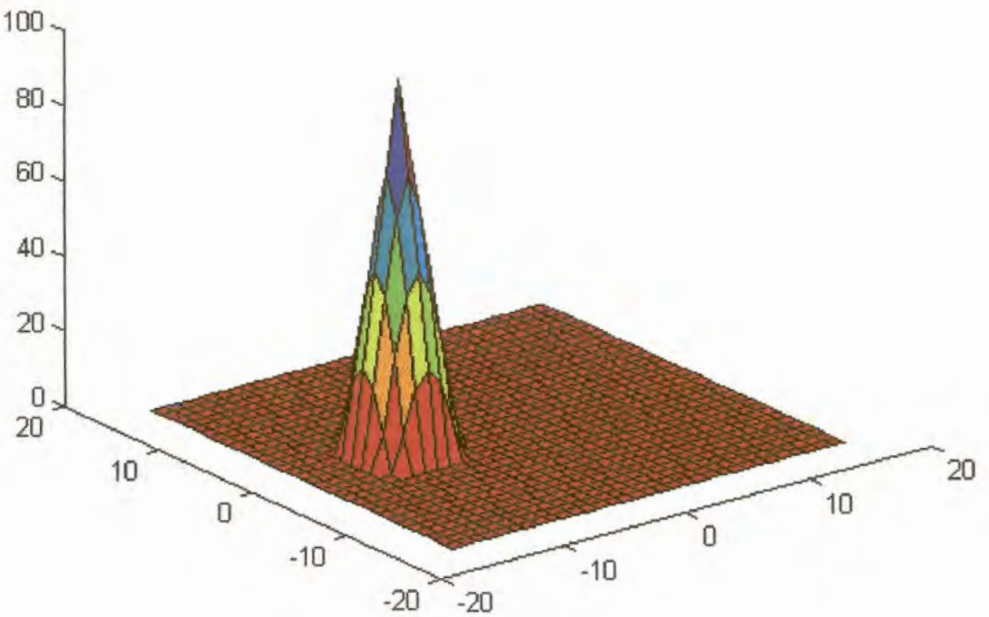

Figure 4.10 Initial cone configuration in 3-dimensions for Crowley's test. The cone has a height of 100 units, base diameter of 8 units and is centred at position (-8,0).

Isotachs (constant wind speed contours) of the constant in time velocity field (black contours) and height level contours which depict the initial cone position are displayed in figure 4.9. The rotation is clockwise and the angular velocity is chosen to be $\Omega = 7.2722$ rads^{-1}. A 3-dimensional representation of the cone in figure 4.9 is displayed in figure 4.10.

Since the evolution of ψ is governed by advection only and the specified velocity field corresponds to solid rotation, it is expected that the cone should migrate in a circle of constant radius in a clockwise direction around the centre of the grid mesh.

In this section the term "integration area" is used to refer to all the inner grid points, in other words, the 31x31 grid points covering the domain where $-15 \le x \le 15, -15 \le y \le 15$. The passive lateral boundary zone where the height of the cone is held zero is therefore excluded from the integration area. Two

complications may develop near the boundary of the integration area during semi-Lagrangian calculations. In the first place the upstream point (x_*, y_*) may be of such a nature that the values of (i, j), which satisfy equation **(4.51)**, fall outside the defined domain. Secondly, even if these points fall inside the domain, some of the points needed to perform the interpolation may fall outside. Following McDonald (1984), a solution to the former complication is to introduce a number of additional passive boundary lines when the field is initially defined. Similar to the passive boundary zone, the height of the cone is kept as zero at the additional boundary points and is never updated during the integration. The number of passive lateral boundary rows is chosen as the smallest integer greater than the maximum possible value of $|\kappa_x|$ or $|\kappa_y|$, where

$$\kappa_x = \sum_{n=1}^{N} \frac{(-\Delta t)^n}{n!} \frac{d^n x}{dt^n} \qquad \text{and} \qquad \kappa_y = \sum_{n=1}^{N} \frac{(-\Delta t)^n}{n!} \frac{d^n y}{dt^n}$$

Here, $N = 1,2,3$ for the D_1, D_2 and D_3 schemes respectively.

The second complication is resolved by performing a bilinear interpolation whenever the bicubic interpolation scheme requires points which fall outside the area of integration plus additional boundary lines.

As long as $|\kappa_x|$ and $|\kappa_y|$ are < 1, only one passive boundary line is required. If values of $|\kappa_x|$ and $|\kappa_y|$ are expected to be less or equal than m (where m is a positive integer), m passive boundary lines must be included. If space is at its premium, the inclusion of additional boundary rows represents a drawback of the semi-Lagrangian schemes, since the size of the arrays has to be increased to accommodate these additional values of the fields.

Figure 4.11a shows the scalar distribution of the cone after one revolution using the Leapfrog scheme with 48 steps per revolution. The associated time step yields that the maximum value of $\frac{c\Delta t}{\Delta x}$ (listed in Table 4.1) is almost four times the maximum value allowed for the CFL criterion (equation **(4.23)**) to be satisfied. Thus, it is not surprising that the solution became unstable (note the dramatic increase in cone height depicted in figure 4.11a).

Figure 4.11b (288 steps per revolution) vividly illustrates other typical problems associated with finite difference approximations of the non-linear advection equation. Although the integration remained stable (the CFL criterion is satisfied in this case, see Table 4.1), large errors in phase and amplitude are present (Table 4.2). Spurious trailing waves can also be observed in the numerical solution (figure 4.11b).

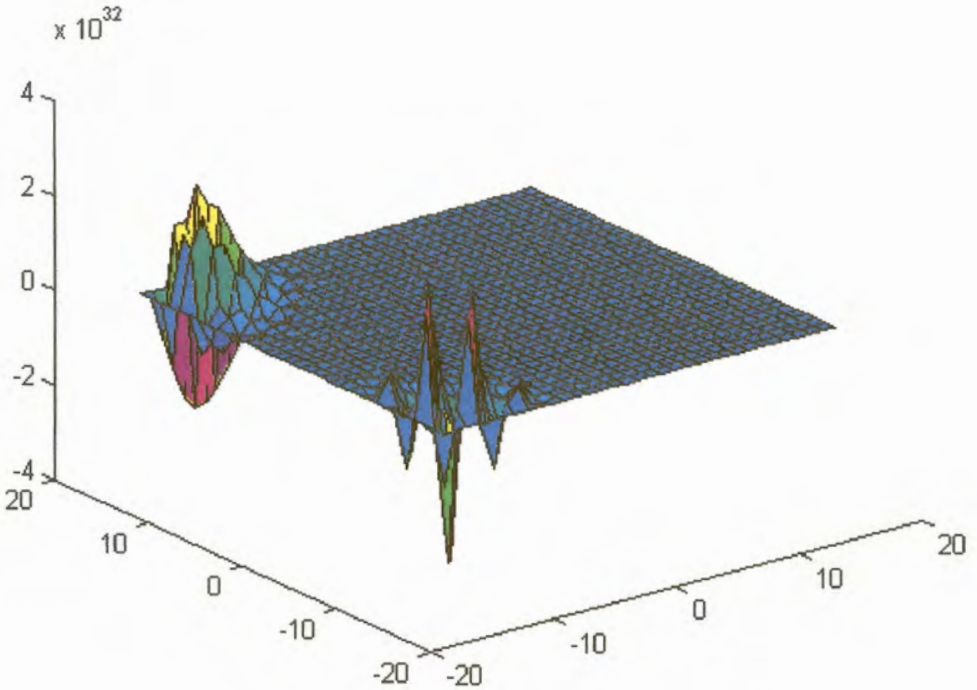

Figure 4.11a The advected scalar field in Crowley's cone test after one revolution (48 steps) with the Leapfrog scheme.

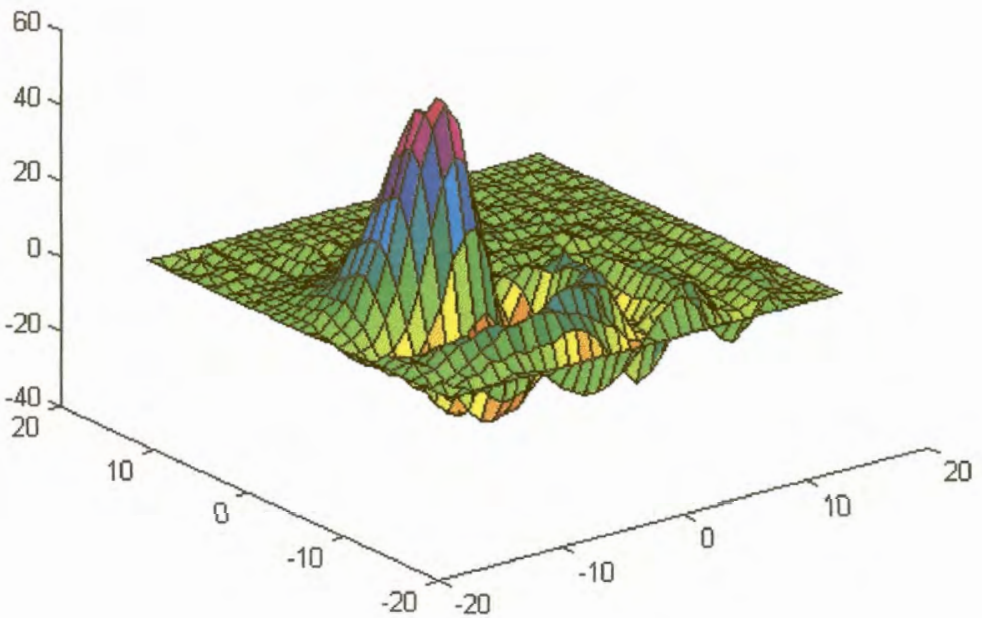

Figure 4.11b The advected scalar field in Crowley's cone test after one revolution (288 steps) with the Leapfrog scheme.

Figures 4.12a and 4.12b show the scalar distribution after one revolution using the Lax-Wendroff and modified Lax-Wendrof schemes respectively with 288 time steps per revolution. The time step yields that the maximum value of $\frac{c\Delta t}{\Delta x}$ (listed in Table 4.1) in the two schemes is less than half the value required to satisfy the CFL criterion (equation **(4.41)**). Figures 4.12a and 4.12b as well as Table 4.2 clearly illustrate that the Lax-Wendroff scheme has damping and phase properties that are inferior to those of the modified Lax Wendroff scheme. Unpleasant trailing waves occur in both integrations, but the amplitudes of these waves are significantly smaller for the modified Lax Wendroff scheme. Conservation properties of the modified Lax-Wendroff scheme are undoubtedly superior to those of the Lax-Wendroff scheme (Table 4.2). Whilst the modified Lax-Wendroff scheme clearly represents an improvement over the Lax-Wendroff (and the Leapfrog) schemes, phase errors may still be problematic.

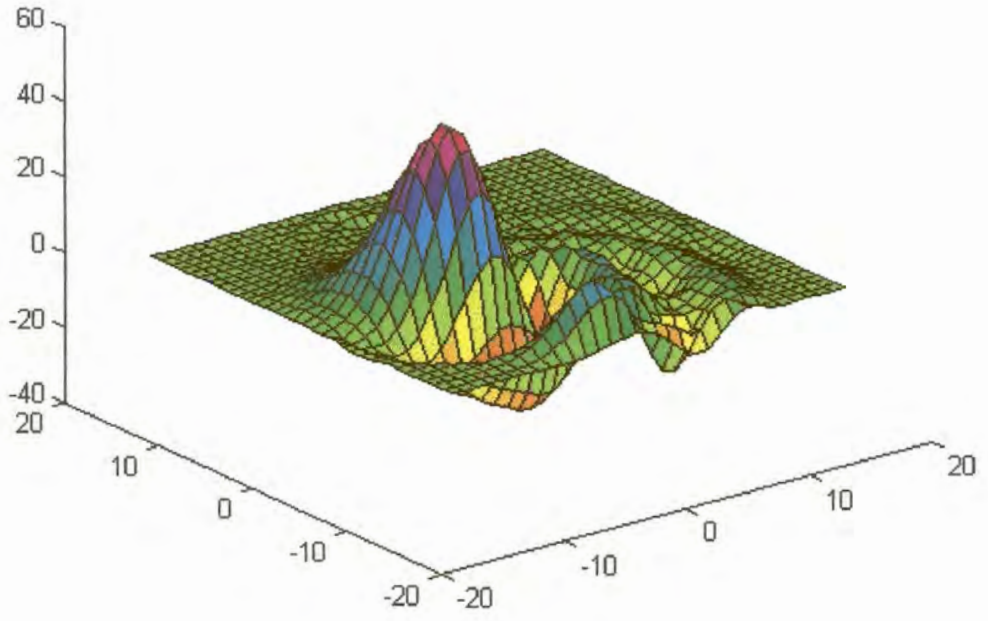

Figure 4.12a The advected scalar field after one revolution (288 steps) with the Lax-Wendroff scheme.

The last column in Table 4.2 also suggests that the Lax-Wendroff scheme has a tendency to artificially enhance the concentration of the advected scalar field.

Both the Lax-Wendroff and modified Lax-Wendroff schemes become unstable when 48 steps are used for one revolution. This comes as no surprise, since the CFL criterion is violated by a factor of almost three (Table 4.1). Note that

in comparison with the Leapfrog and semi-Lagrangian schemes, the quantity $c\frac{\Delta t}{\Delta x}$ attains larger magnitudes (for this specific velocity field) when the two Lax-Wendroff schemes are used. This is due to caculations performed at the outer "half-points" during integrations with the two Lax-Wendroff schemes.

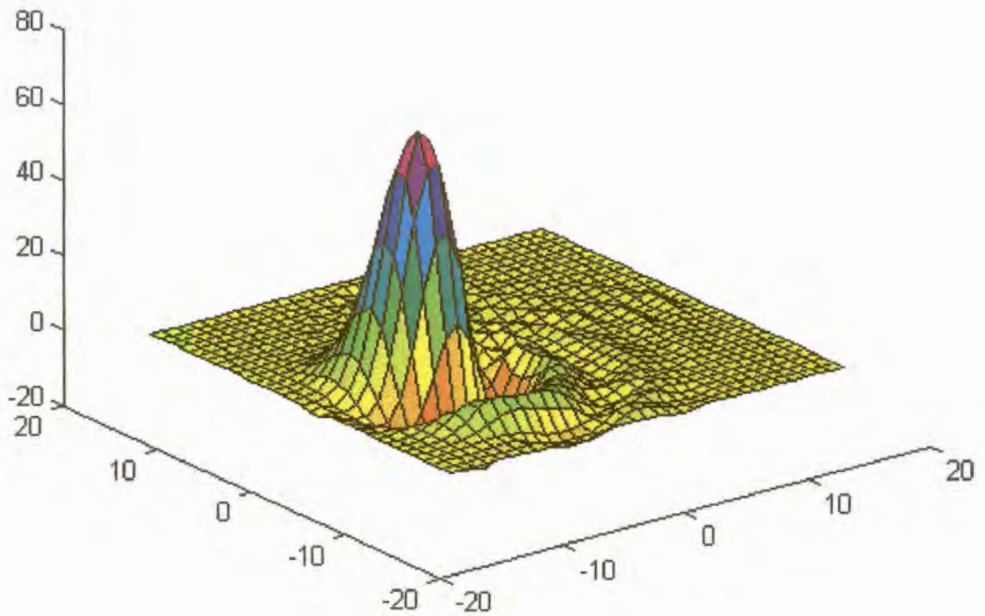

Figure 4.12b The advected scalar field after one revolution (288 steps) with the modified Lax-Wendroff scheme.

Scheme	Number of time steps per revolution	$c\frac{\Delta t}{\Delta x}$	Number of passive boundary lines needed
Leapfrog	48	2.777	1
	288	0.463	1
Lax-Wendroff	48	2.869	1
	288	0.478	1
Modified	48	2.869	2
Lax-Wendroff	288	0.478	2
D1, D2 and D3	48	2.777	3
	288	0.463	1

Table 4.1. Maximum values of $c\frac{\Delta t}{\Delta x}$ and the number of passive boundary lines required for the various schemes expressed as a function of the amount of time steps used per revolution in Crowley's cone test.

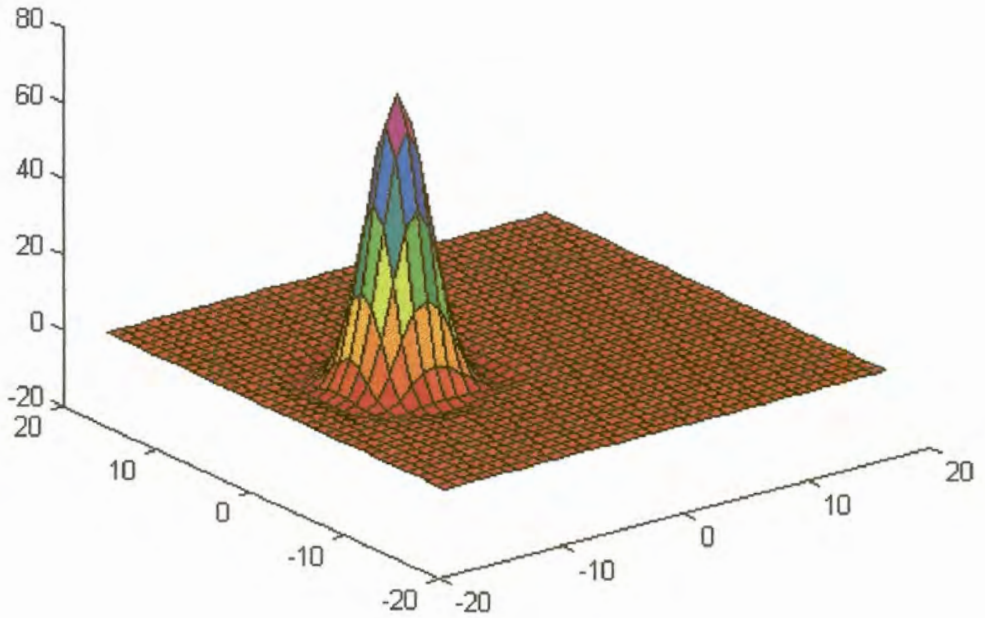

Figure 4.13a The advected scalar field after one revolution (48 steps) with the D_3 scheme.

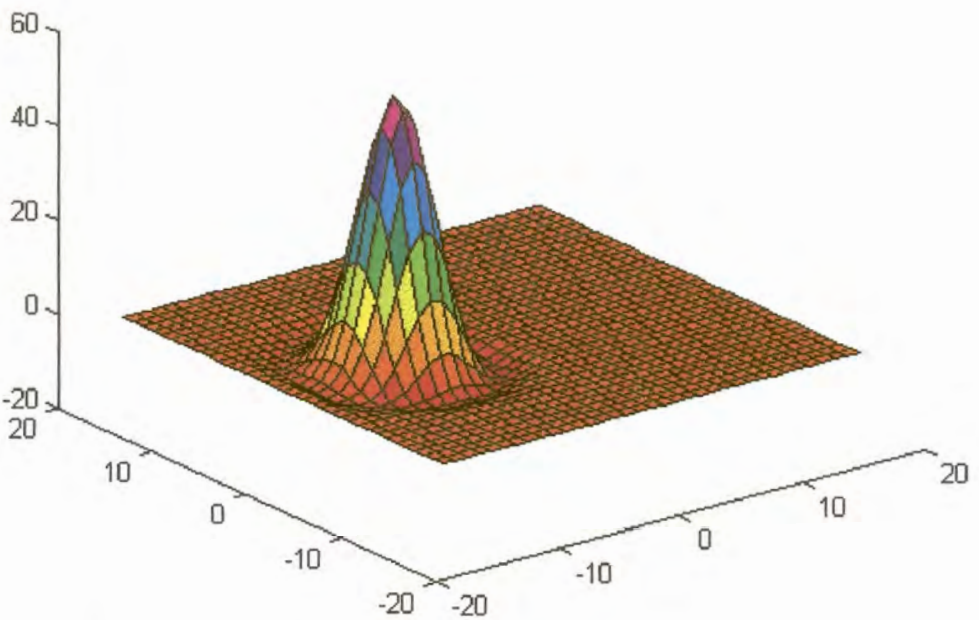

Figure 4.13b The advected scalar field after one revolution (288 steps) with the D_3 scheme.

The position and symmetry of the scalar distribution after one revolution using 48 steps (figure 4.13a) or 288 steps (figure 4.13b) are excellent for the D_1, D_2 and D_3 schemes. The figures are for the D_3 scheme. Some smoothing of the profile is however evident for smaller time steps (Table 4.2). The height errors for the higher-order semi-Lagrangian schemes (Table 4.2) are least when larger time steps are used. This may be attributed to the smaller number of interpolations performed at each revolution (McGregor, 1993). Note that the semi-Lagrangian schemes remain stable (Table 4.2) when 48 steps per revolution is used, despite the fact that the CFL criterion is violated by a factor of almost three (Table 4.1).

Scheme	Number of itera-tions	Maxi-mum height	Mini-mum height	Distan-ce error	Angular error in degrees	$\frac{\sum \psi_{ij}}{\sum \psi_{ij}(0)}$	$\frac{\sum \psi_{ij}^2}{\sum \psi_{ij}^2(0)}$	$\frac{\sum \lvert\psi_{ij}\rvert}{\sum \lvert\psi_{ij}(0)\rvert}$
Leapfrog	288	56.8	-22.3	-0.384	-23.2	1.013	1.002	2.602
	2*288	56.3	-22.2	-0.384	-23.2	1.014	1.001	2.613
	4*288	56.3	-22.1	0.062	-29.7	1.014	1.000	2.616
	10*288	56.3	-22.1	0.062	-29.7	1.015	1.000	2.616
Lax-Wendroff	288	48.9	-20.6	0.062	-29.7	1.005	0.867	2.429
	2*288	49.1	-21.7	0.062	-29.7	1.006	0.919	2.613
	4*288	49.3	-22.2	-0.384	-23.2	1.007	0.955	2.743
	10*288	49.6	-22.8	0.062	-29.7	1.008	0.983	2.862
Modified	288	67.5	-16.6	-0.250	-14.0	1.000	0.914	1.749
Lax-Wendroff	2*288	73.7	-14.7	0.062	-7.1	1.002	0.957	1.640
	4*288	76.0	-14.8	0.062	-7.1	1.004	0.976	1.648
	10*288	76.7	-15.4	0.062	-7.1	1.008	0.989	1.704
D_1	48	58.5	-2.0	-3	0	0.442	0.317	0.517
	288	54.2	-2.5	-1.0	0	0.868	0.577	1.052
	2*288	53.9	-2.5	0	0	0.932	0.619	1.126
	4*288	54.5	-2.6	0	0	0.965	0.641	1.163
	10*288	54.7	-2.6	0	0	0.987	0.655	1.186
D_2	48	74.6	-1.5	0	0	0.995	0.847	1.099
	288	56.4	-2.3	0	0	1.000	0.678	1.191
	2*288	55.5	-2.4	0	0	1.000	0.671	1.196
	4*288	55.1	-2.5	0	0	1.001	0.668	1.199
	10*288	55.0	-2.5	0	0	1.001	0.666	1.200
D_3	48	76.9	-1.5	0	0	1.000	0.852	1.102
	288	56.4	-2.3	0	0	1.000	0.678	1.191
	2*288	55.5	-2.4	0	0	1.000	0.671	1.196
	4*288	55.2	-2.5	0	0	1.001	0.668	1.199
	10*288	55.0	-2.6	0	0	1.001	0.666	1.200

Table 4.2. Maximum height, minimum height, radial error in units of grid lengths, angular error in degrees, and conservation properties after one revolution of Crowley's cone test are shown for various schemes. Initially the maximum height is 100 and the minimum is zero.

The D_2 and D_3 schemes are superior to the D_1 scheme since they have smaller height errors, better phase representation and better conservation properties (Table 4.2). The D_3 scheme produces superior results to the D_2 scheme with respect to reduced height errors and improved conservation properties, especially for larger time steps (Table 4.2).

The conservation properties $\frac{\sum \psi_{ij}}{\sum \psi_{ij}(0)}$ and $\frac{\sum |\psi_{ij}|}{\sum |\psi_{ij}(0)|}$ are excellent (Table 4.2) in the D_2 and D_3 schemes. However, the conservation property $\frac{\sum \psi_{ij}^2}{\sum \psi_{ij}^2(0)}$ (Table 4.2) is relatively low (compared to the values obtained for the two Lax-Wendroff schemes) for the semi-Lagrangian schemes. This may be attributed to the bicubic interpolation procedure used at each time step, which spuriously spreads the scalar field over an artificially large region. When the small values at each grid point are squared during the calculation of the conservation property $\frac{\sum \psi_{ij}^2}{\sum \psi_{ij}^2(0)}$, relatively low values are obtained. When smaller time steps are used the effect becomes even more apparent (Table 4.2) because more bicubic interpolations are performed. This represents a further drawback of the semi-Lagrangian schemes, despite the fact that the scalar field is conserved finely.

Figures 4.13a, 4.13b and Table 4.2 suggest that the D_1, D_2 and D_3 schemes are superior to the modified Lax-Wendroff scheme with respect to the occurrence of phase errors. The unpleasant trailing waves present in the Lax-Wendroff simulations are absent in the semi-Lagrangian results. Analysis of the height error in Table 4.2 suggests that the modified Lax-Wendroff scheme preserves the cone height. However, it wrongly creates large negative values for the scalar field (minimum height in Table 4.2). The conservation property $\frac{\sum |\psi_{ij}|}{\sum |\psi_{ij}(0)|}$ indicate that the modified Lax-Wendroff scheme falsely increases the scalar concentration. In this respect the modified Lax-Wendroff scheme is undoubtedly inferior to the D_2 and D_3 schemes.

4.5.2 STRONG DEFORMATIONAL FLOW: SMOLARKIEWICZ'S TEST

As long as the modified Lax Wendroff scheme is applied to a constant velocity field or to smooth non-deformational flow (such as the flow field defined in Crowley's cone test), it provides reasonable results. For deformational flow however, significant differences exist between the behaviour of the modified Lax-Wendroff and the semi-Lagrangian schemes. It is difficult to prove stability of a scheme under conditions of non-uniform flow, since stability features may depend on the structure of the velocity field. Therefore a fixed chosen example, which involves strong deformational flow will be used in this study to

evaluate the properties of the various schemes under conditions of non-uniform flow.

Smolarkiewicz (1982) defined an interesting deformational flow pattern to evaluate the performance of his multidimensional generalisation of the Crowley (1968) advection scheme. The challenge is to capture the advection properties of a scalar distribution (initially a cone of height 1 unit and base radius 15 units centred on a square domain with a boundary dimension of $L = 100$ units) in a flow field defined by the stream function:

$$\phi(x, y) = A \sin(kx)\cos(ky)$$

where $A = 8$, $k = \frac{4\pi}{L}$ and the position of the central point on the square is $x = y = 50$. This is also the position of the centre of the initial cone distribution.

The equation for the initial scalar distribution is

$$\psi(x, y) = -\left(\frac{1}{15}\right)\sqrt{(x-50)^2 + (y-50)^2} + 1; \quad (x-50)^2 + (y-50)^2 \le 15^2$$

and the velocity field is given by

$$\bar{v} = \left(-\frac{\partial\phi}{\partial y}, \frac{\partial\phi}{\partial x}\right) = [Ak \sin(kx)\sin(ky), Ak \cos(kx)\cos(ky)]$$

Following Smolarkiewicz (1982), $\Delta t = 0.7$ s is chosen, implying that $c\frac{\Delta t}{\Delta x} = 0.7$. Deformation of the velocity field is defined as (Smolarkiewicz, 1982):

$$Def \equiv \frac{\partial u}{\partial x} - \frac{\partial v}{\partial y}.$$

As a result of the inequality $Max(Def)\Delta t = 1.4 > 1$, deformation can be considered as strong (Smolarkiewicz, 1982).

Isolines of the stream function (blue and green lines) and height level lines of the initial scalar distribution (red contours) are illustrated in figure 4.14. The initial scalar distribution is displayed in three-dimensions in figure 4.15. The velocity field is constructed in terms of a set of square boxes with symmetrical vortices. Rotation in the blue vortices in figure 4.14 is clockwise while the green vortices represent counter-clockwise rotation. Each vortex occupies a square of side length 25 units.

The radius of the base of the cone is slightly greater than the radius of the vortices (figure 4.14), so that at the initial time the cone distribution covers areas in six vortices. It is expected that the solution, after a long enough integration period, will be of such a nature that two symmetrical pieces of the cone will move into the area of the two central vortices (Smolarkiewicz, 1982).

Staniforth et al. (1987), pointed out that fluid elements are constrained to move along the streamlines for this problem and cannot escape from the vortex in which they are found at the initial point in time (because they cannot cross the bounding streamline of the vortex). Since the initial scalar distribution is nonzero over six vortexes, it will be nonzero over these six vortexes for all time. A second consequence of this property of fluid elements is that for each of the four peripheral vortices the solution should be identically zero everywhere inside the streamline that is tangent to the base of the cone at initial time (see figure 4.14). Thus, for each of these four vortices the nonzero part of the solution is confined to a narrow region close to its boundary.

Corners and centres of vortices are stagnation points of the flow. The corners are saddle points of the stream function, whereas the centres are local extrema. The solution of the advection problem at any stagnation point retains its initial value for all time intervals. However fluid elements in an infinitesimally small neighbourhood of saddle points are transported along their initial streamline and replaced by an upstream fluid element carrying a different value of the scalar field. Consequently, an increasing gradient in the scalar distribution develops at saddle points (Staniforth et al., 1987).

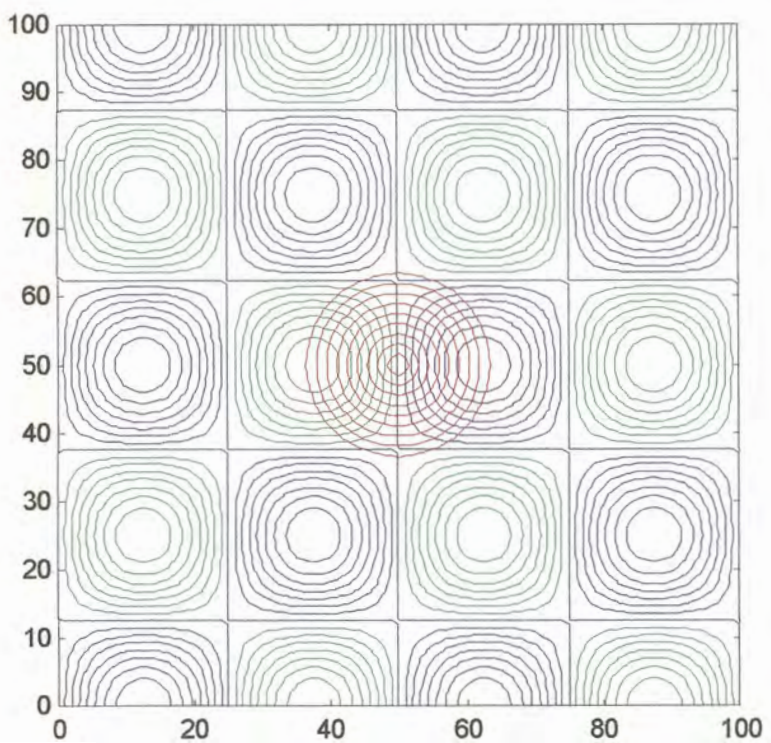

Figure 4.14 Isolines of the streamfunction for Smolarkiewicz's test with the initial scalar distribution (red contours) in the form of a cone of height 1 unit and base diameter 30 units superimposed. Rotation of the blue vortices is clockwise while the green vortices represent counter-clockwise rotation.

There have been attempts to find the analytic solution of Smolarkiewicz test problem. Staniforth et al. (1987) illustrated that when the position of a fluid element at time t_0 is known, its position at time t may be found in terms of Jacobian elliptic functions. Since the quantity ψ is conserved along a trajectory, ψ can be predicted at time t, as long as ψ is known at $t = t_0$ (Staniforth et al., 1987). However, Leonard et al. (1996) point out that the solution presented by Staniforth et al. (1987) deals with nodal-point values on a highly variable grid with drastically increased resolution in regions of large gradient in the advected field. Instead of working with this analytic solution, Leonard et al. (1996) preferred to use a highly accurate fourth-order Runge-Kutta scheme with a small time step to find the initial position (and hence the initial ψ value) of a fluid element located at position (x_1, y_1) at time t. In this section the results of the various schemes will be evaluated against the expected qualitative behaviour of the true solution.

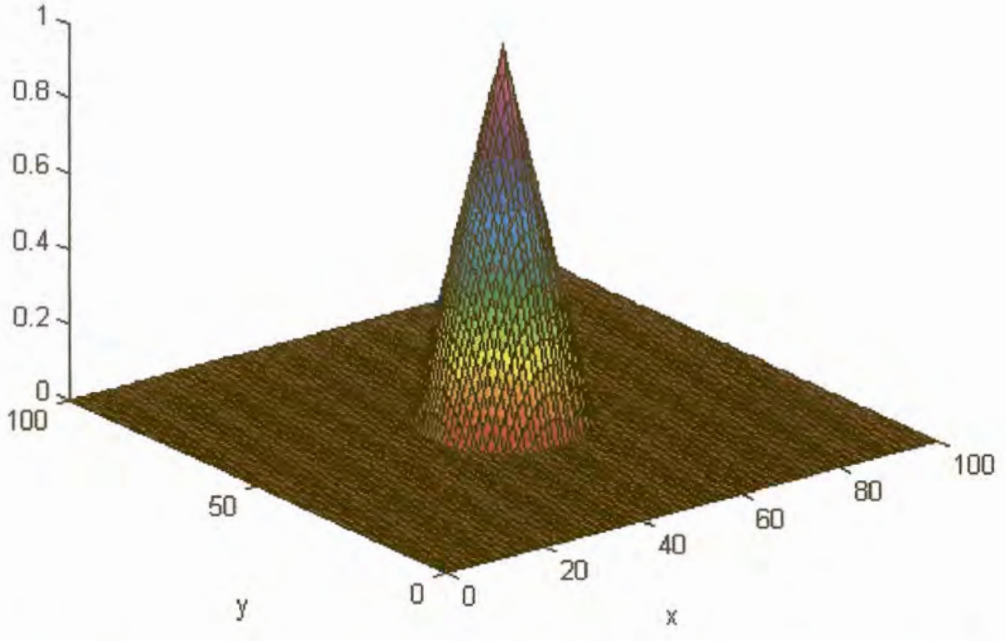

Figure 4.15 Initial cone configuration in 3-dimensions for Smolarkiewic's test. The cone has a height of 1 unit, base diameter of 30 units and is centred at position (50,50).

The numerical solutions obtained after 19, 38, 57, 75, 377 and 3768 iterations (using $\Delta t = 0.7$ s) with the D_3 scheme are displayed in figures 4.16a to 4.16f. respectively. The number of iterations given above closely correspond to the times t=T/200, t=T/100, t=3T/200, t=T/50, t=T/10 and t=T where T=2637.6 s is the final time of integration used by Smolarkiewicz (1982). Staniforth et al. (1987) give presentations of the analytical solution of Smolarkiewicz's problem at these time steps.

In figure 4.16a it can be seen that the scalar distribution inside each of the two "main vortexes" starts to rotate about the vortex centres. Maximum quantities move away from the domain centre towards the stagnation points in the positive y direction. The distribution has a left/right symmetry. The behaviour of the numerical solution in figure 4.16a (after 19 iterations) is thus in complete harmony with the expected qualitative behaviour of the true solutions that was discussed earlier.

The fragments of the cone that were initially inside the four peripheral vortices move along their trajectories near the perimeter (figure 4.16b, 38 iterations). Simultaneously, a strong gradient in the scalar distribution is developing near the saddle points of the two "main vortices". Figure 4.16c (57 iterations) reveals the first qualitative difference between the numerical solution and the true solution: Negative scalar quantities exist in the numerical solution (black contours in figure 4.16c). Negative weights used in the bicubic interpolation procedure possibly contribute to this defect in the numerical solution.

After 75 iterations (figure 4.16d) the negative scalar distribution in the numerical simulation has increased slightly. The fact however, that the true solution remains confined to the six vortexes that contained the initial cone distribution and the fact that the scalar distribution cannot cross the bounding streamlines, are well represented in the simulation with the D_3 scheme. The scalar quantity starts to spiral in towards the centres of the two main vortexes.

In figure 4.16e the scalar distribution is divided into two symmetrical pieces, with maximum concentrations located within the two "main vortexes", as can be expected. Although this pattern is still preserved in figure 4.16f there is a sudden outbreak of negative scalar quantities over some of the peripheral vortexes. The negative quantities also succeeded in crossing the bounding streamlines and intruding into the centres of some of the peripheral vortexes, which is inconsistent with the expected qualitative behaviour of the true solution.

The numerical solution depicted in figures 4.16a to 4.16f closely corresponds to the analytical solution presented by Staniforth et al. (1986). The solution remains stable although some of the scalar distribution eventually escapes into the peripheral vortices (figure 4.16f). The D_1 and D_2 schemes qualitatively illustrate the same behaviour as the D_3 scheme (not shown). The conservation properties of the D3 scheme are slightly superior to that of the D_2 scheme (Table 4.3). The conservation properties of the D_1 scheme are inferior to those of the D_2 and D_3 schemes for all cases expect for the final case of 3768 iterations in Table 4.3. The two latter schemes spuriously create more of the scalar quantity when $t \rightarrow T$, especially in the form of negative quantities intruding some of the peripheral vortices (figure 4.6bf). The reason for this interesting behaviour (and why it is absent in the D_1 solution) is not presently known.

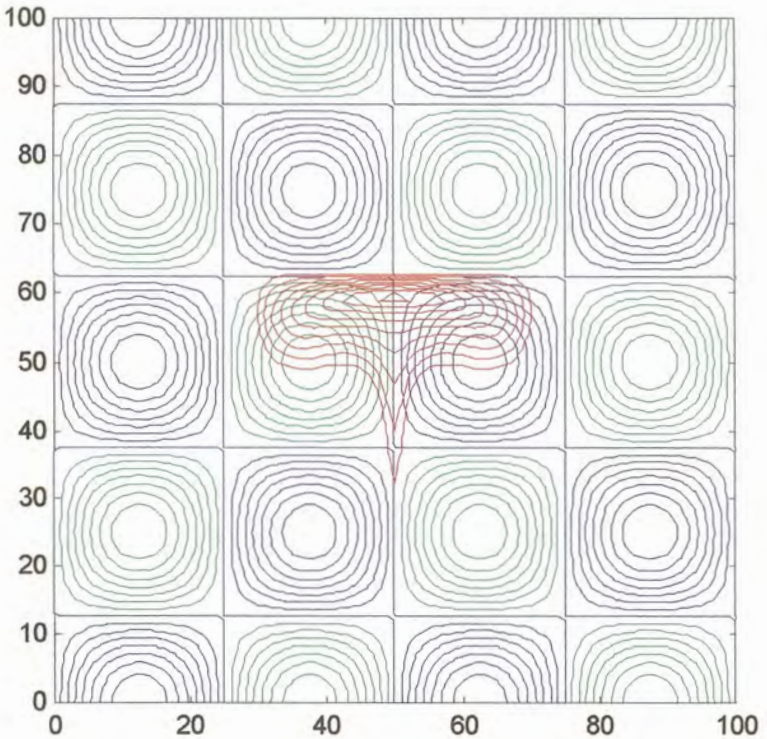

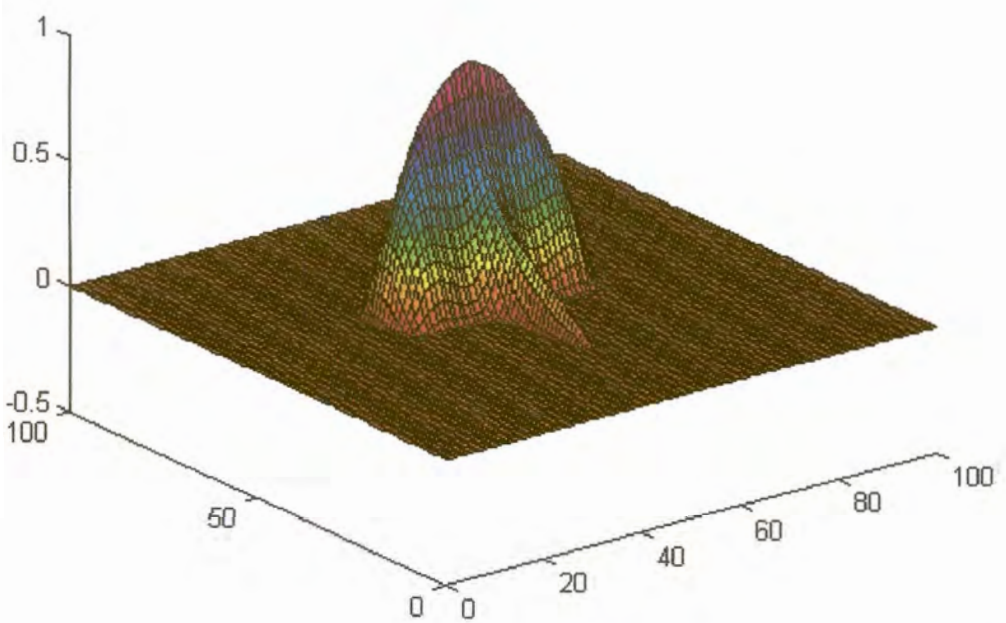

Figure 4.16a The scalar distribution in Smolarkiewicz's deformational flow after 19 iterations (Δt=0.7 s) with the D_3 scheme.

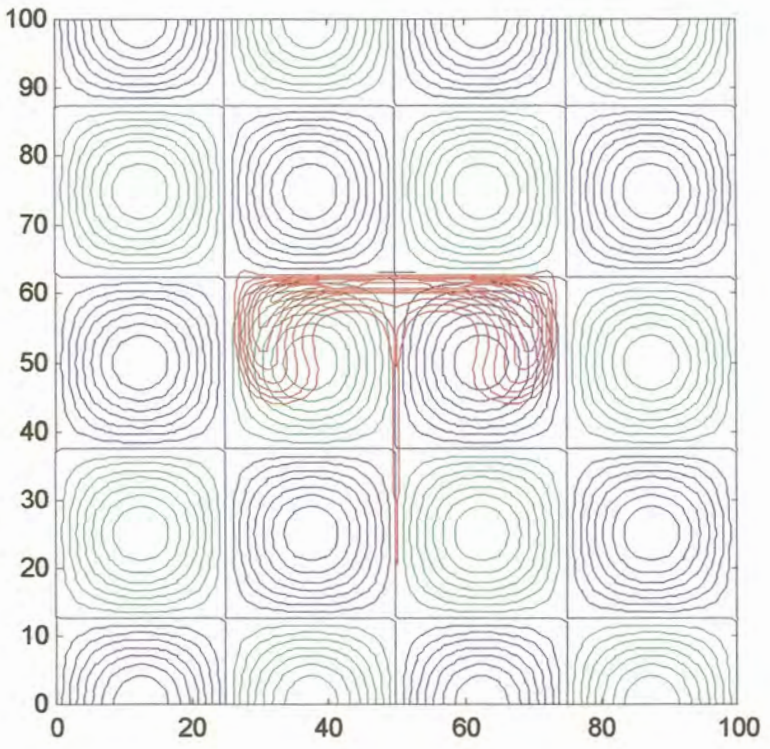

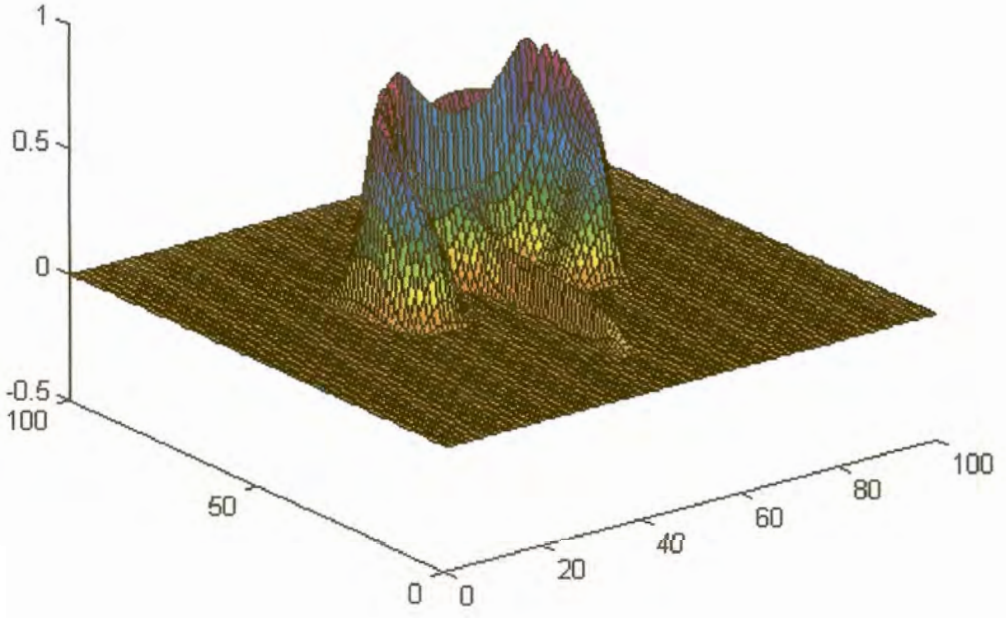

Figure 4.16b The scalar distribution in Smolarkiewicz's deformational flow after 38 iterations (Δt=0.7 s) with the D_3 scheme.

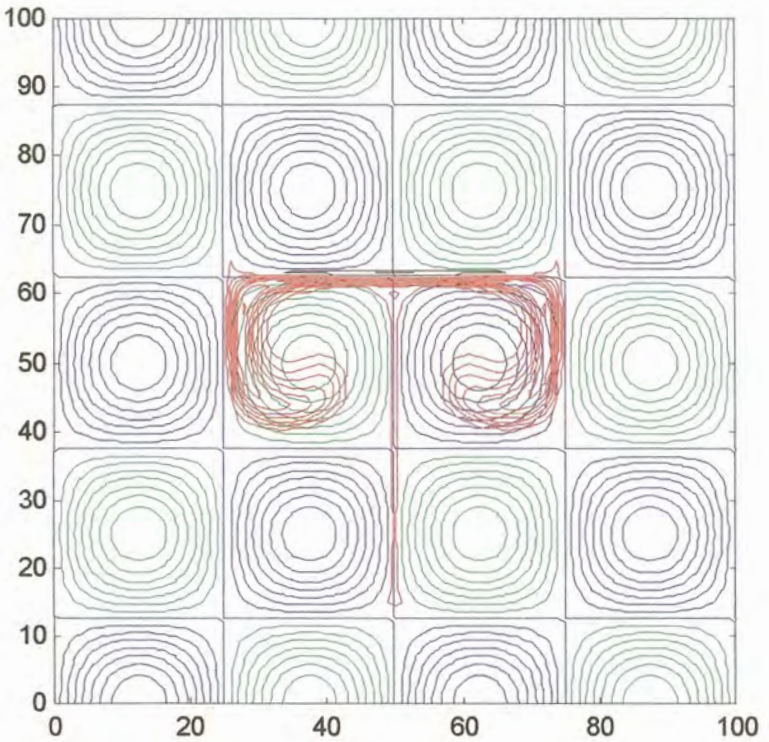

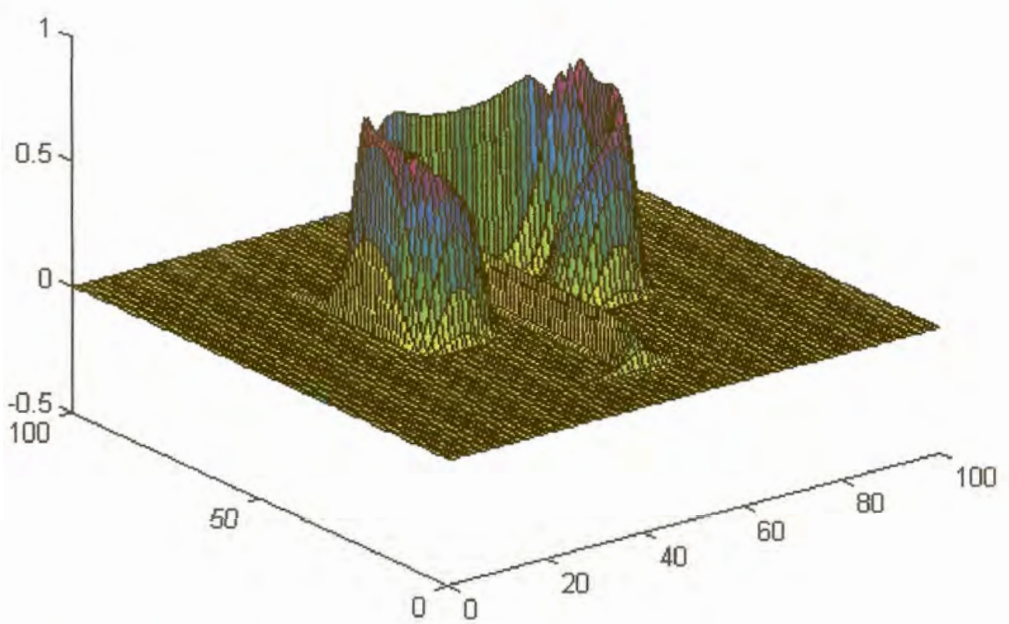

Figure 4.16c The scalar distribution in Smolarkiewicz's deformational flow after 57 iterations (Δt=0.7 s) with the D_3 scheme.

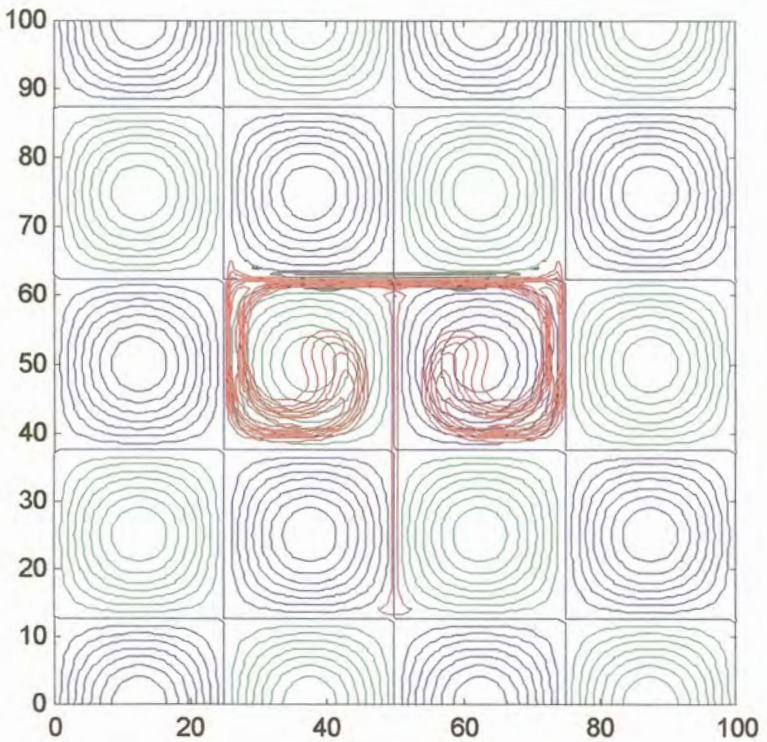

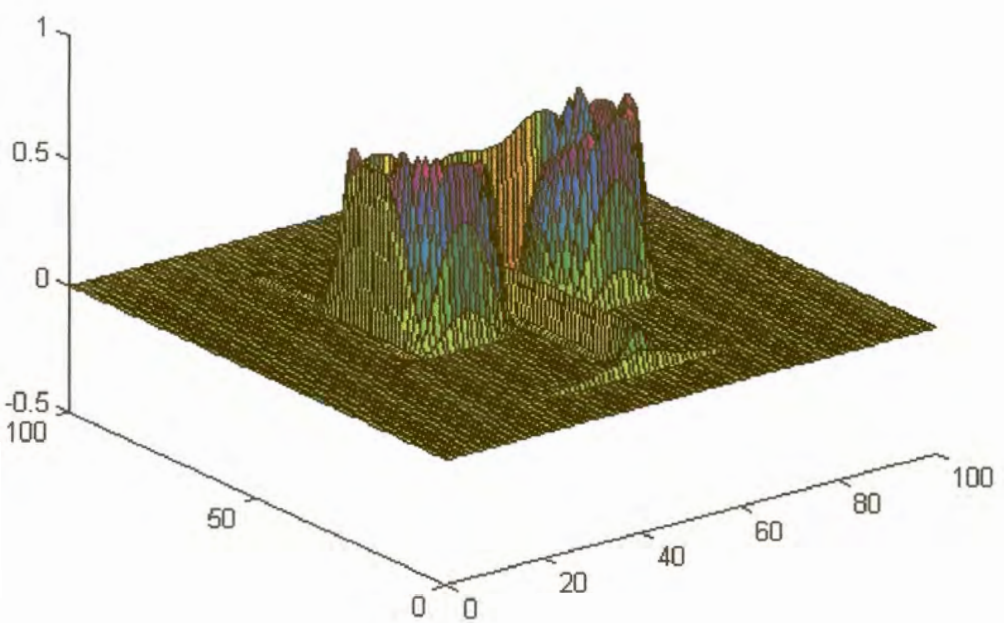

Figure 4.16d The scalar distribution in Smolarkiewicz's deformational flow after 75 iterations (Δt=0.7 s) with the D_3 scheme

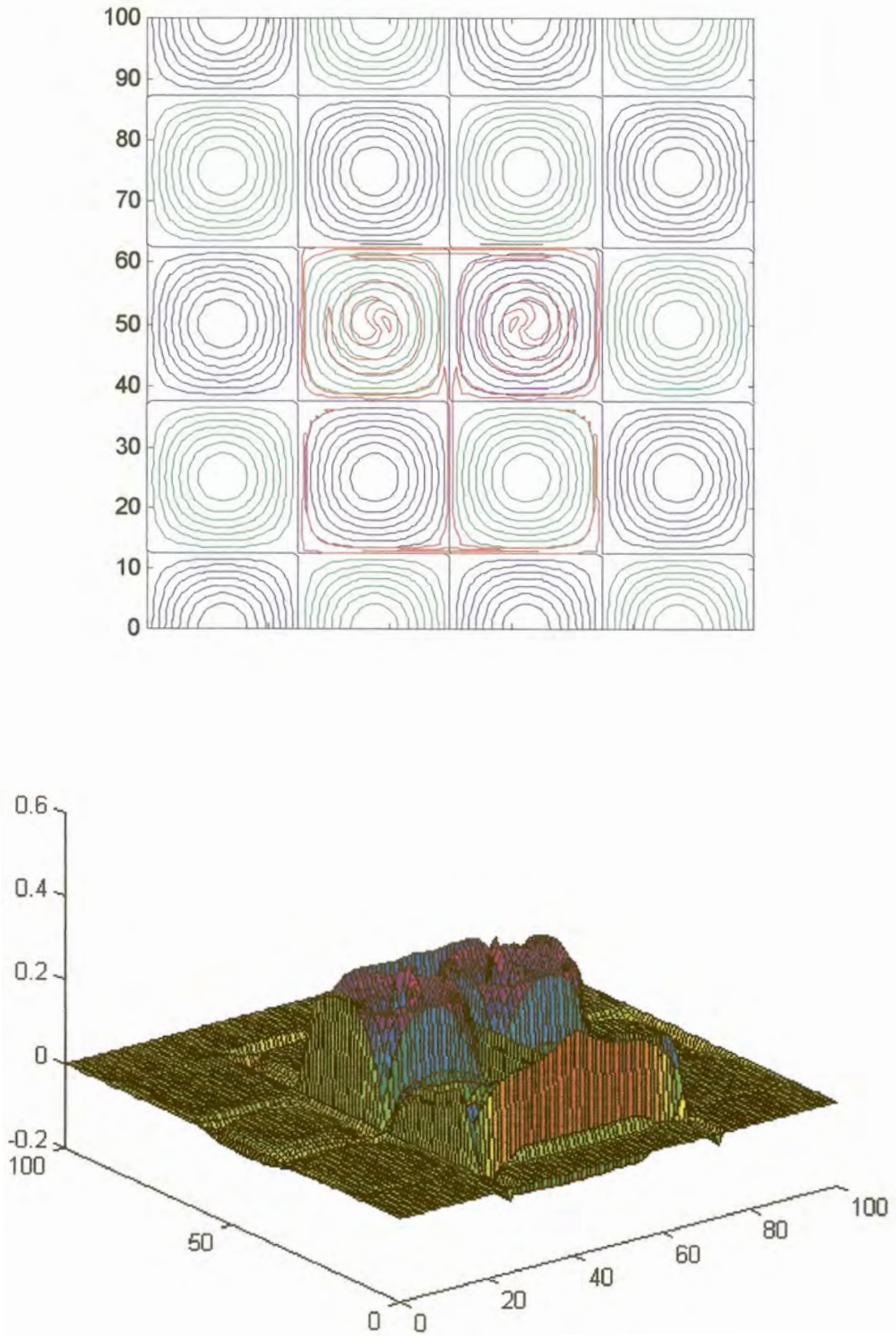

Figure 4.16e The scalar distribution in Smolarkiewicz's deformational flow after 377 iterations (Δt=0.7 s) with the D_3 scheme

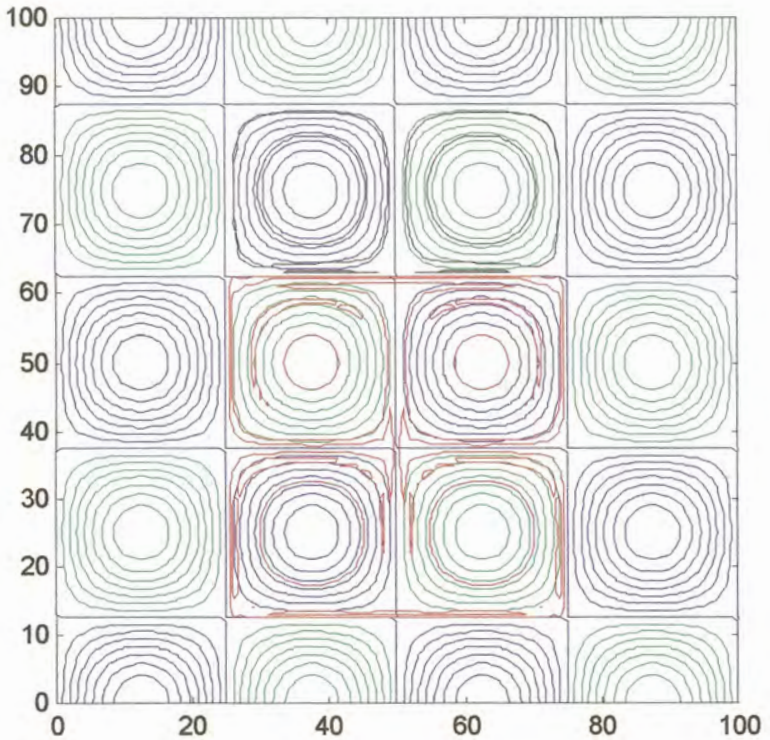

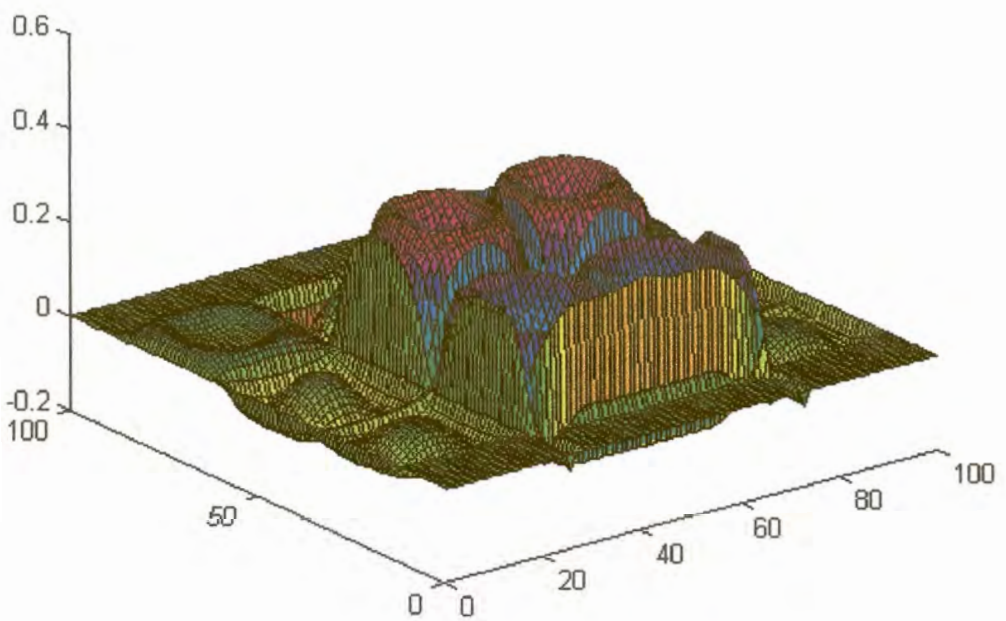

Figure 4.16f The scalar distribution in Smolarkiewicz's deformational flow after 3768 iterations (Δt=0.7 s) with the D_3 scheme

The Leapfrog scheme and both Lax-Wendroff schemes spectacularly fail Smolarkiewicz's test. After only 57 iterations, growing instabilities can be observed in the numerical solutions of all three these schemes. This can be seen from the conservation property $\frac{\sum|\psi_{ij}|}{\sum|\psi_{ij}(0)|}$ in Table 4.3, which for all three finite difference schemes rapidly increases as time increases. The instabilities grow exceptionally fast in the numerical solution of the Leapfrog scheme.

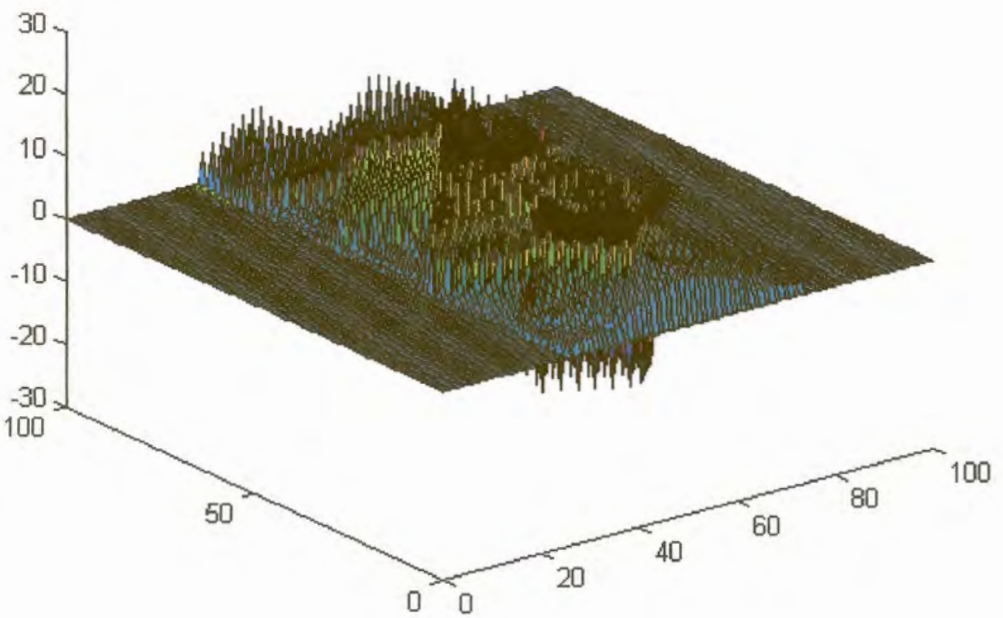

Figure 4.17 The scalar distribution in Smolarkiewicz's deformational flow after 377 iterations (Δt=0.7 s) with the leapfrog scheme.

Figure 4.17 show the solution obtained from the leapfrog scheme after 377 iterations. Figure 4.18 shows the corresponding solution produced by the modified Lax-Wendroff scheme. The solution obtained from the Lax-Wendroff scheme (not shown) is qualitatively similar to that of the modified Lax-Wendroff scheme. Conservation properties of the Lax-Wendroff scheme are only slightly inferior to those of the modified Lax-Wendroff scheme (Table 4.3). For Smolarkiewicz's test (strong deformational flow) the modified Lax-Wendroff scheme does not offer significant advantages over the computationally more efficient Lax-Wendroff scheme. In contrast to the finite

Scheme	Number of iterations	$\frac{\sum \psi_{ij}}{\sum \psi_{ij}(0)}$	$\frac{\sum \psi_{ij}^2}{\sum \psi_{ij}^2(0)}$	$\frac{\sum \lvert\psi_{ij}\rvert}{\sum \lvert\psi_{ij}(0)\rvert}$
Leapfrog	19	1.000	1.014	1.034
	38	1.000	1.097	1.164
	57	1.000	1.466	1.671
	75	1.000	2.576	2.719
	377	6.107	1936.076	109.665
	3768	Unstable	Unstable	Unstable
Lax-Wendroff	19	1.000	1.007	1.022
	38	1.000	1.042	1.081
	57	1.000	1.123	1.255
	75	1.000	1.320	1.530
	377	0.959	2.478	3.156
	3768	0.861	26.58	12.401
Modified	19	1.000	1.007	1.022
Lax-Wendrof	38	1.000	1.041	1.081
	57	1.000	1.123	1.255
	75	1.000	1.321	1.530
	377	0.959	2.476	3.154
	3768	0.862	26.946	12.519
D_1	19	1.001	1.008	1.010
	38	1.004	1.025	1.041
	57	1.012	1.076	1.122
	75	1.017	1.081	1.199
	377	1.016	0.468	1.526
	3768	1.028	0.446	1.873
D_2	19	1.000	0.998	1.009
	38	1.002	1.009	1.043
	57	1.009	1.060	1.125
	75	1.013	1.058	1.200
	377	1.015	0.493	1.407
	3768	1.154	0.961	2.792
D_3	19	1.000	0.999	1.009
	38	1.002	1.010	1.043
	57	1.009	1.061	1.125
	75	1.013	1.058	1.200
	377	1.015	0.493	1.407
	3768	1.151	0.954	2.780

Table 4.3 Conservation properties of various schemes for Smolarkiewic's test, expressed as a function of the number of iterations (Δt=0.7 s).

difference schemes, the D_N schemes all remain stable during the integration. Compared to the finite difference schemes, the conservation properties of the D_N schemes (in Table 3) are excellent. For Smolarkiewicz's test of strong deformational flow the D_N schemes are by far superior over the finite difference schemes studied.

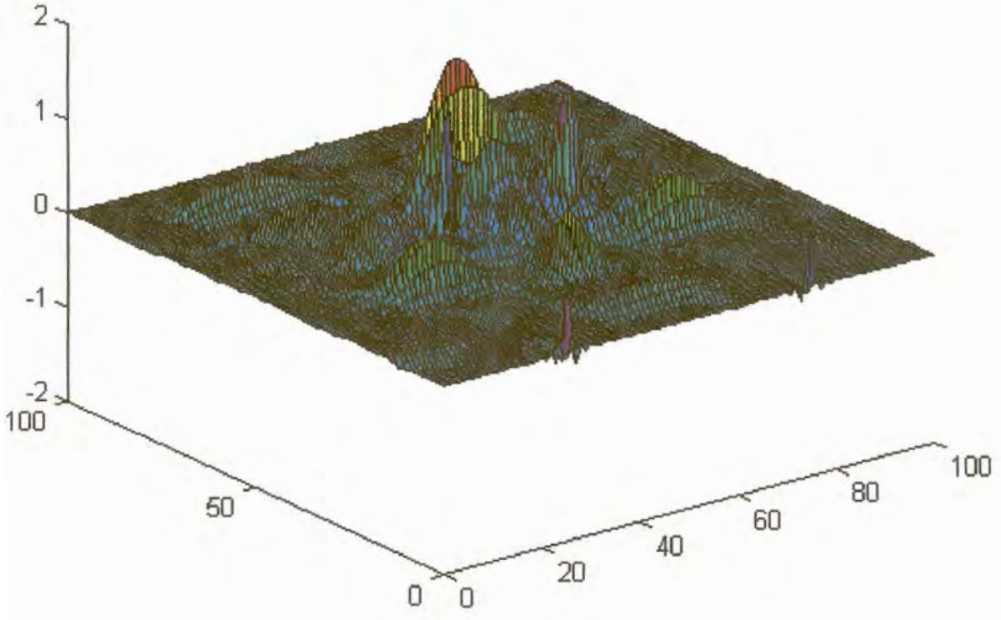

Figure 4.18 The scalar field in Smolarkiewicz's deformational flow after 377 iterations (Δt=0.7 s) with modified Lax-Wendroff scheme.